The Pennsylvania State University

The Graduate School

College of Engineering

ANOMALOUS STREAM TEMPERATURE RESPONSE TO STORMS IN A FORESTED HEADWATER STREAM IN CENTRAL PENNSYLVANIA

A Thesis in

Civil Engineering

by

Katelyn Gerecht

Submitted in Partial Fulfillment
of the Requirements
for the Degree of

Master of Science

August 2012

The thesis of Katelyn Gerecht was reviewed and approved* by the following:

Michael Gooseff
Associate Professor of Civil and Environmental Engineering
Thesis Advisor

Kamini Singha
Associate Professor of Geosciences

Thorsten Wagener
Associate Professor of Civil and Environmental Engineering

Peggy Johnson
Professor of Civil and Environmental Engineering
Head of the Department of Civil and Environmental Engineering

*Signatures are on file in the Graduate School

ABSTRACT

Contrary to previous investigations of stream temperature response to storms in forested headwater streams, we observed sharp increases of up to 3.8 °C in response to storm events in a small 1.5 km^2 watershed that is more than 90% forested. Stream temperature data collected from April through September of 2011 show that during storm events this headwater stream can exhibit a more urban-like stream temperature response. Sudden temperature increases of this magnitude may have negative impacts on the stream's ecological and biogeochemical services. There is a statistically significant difference in the stream's mean temperature response to storms during spring months versus during fall months, suggesting a seasonal relation. The largest and most intense storms between April and June cause the largest increases in stream temperature, while the largest and most intense storms between July and September cause the largest decreases in stream temperature.

We investigate the physical mechanisms of the stream's response to a large storm in May to better understand the cause of the rapid temperature increases. We conclude that climatic variables in this humid climate zone during the spring months cause the precipitation temperature to be much warmer than the pre-storm stream temperature. Low permeability soils and high intensity precipitation cause fast overland runoff to carry this warm "new" water to the stream causing the unexpected temperature anomaly.

We propose that a new conceptual model for explaining storm response in small forested watersheds may be applicable here. Previous research has shown that the bulk of storm response in headwater streams is "older" groundwater being displaced into the stream by the "new" precipitation infiltrating into the subsurface. Instead, here we show that both stream temperature and fluid electrical conductivity observations suggest that the water input to this

stream is primarily “new” water directly from the storm. We see both a freshening and a warming of the stream, whereas if the predicted conceptual model applied to this system we would expect to see the stream cool with an increase in fluid electrical conductivity.

TABLE OF CONTENTS

LIST OF FIGURES

LIST OF TABLES

ACKNOWLEDGMENTS

I would first like to acknowledge my advisors Michael Gooseff and Kamini Singha for the opportunities they provided me at Penn State and for their guidance and support. I also thank Thorsten Wagener for his time and effort while serving on my master's committee. Christa Kelleher gave encouragement and excellent advice, as well as help with the numerical modeling for this project. Even though she is long-distance, Audrey Sawyer continues to provide much needed mentoring and perspective.

I would also like to thank the following people for all of their help both at our field site and at Penn State: Michael Fitzgerald, Tony Moscatello, Tom Voltz, Sarah Godsey, Chris Bakey, Ryan Swanson, Adam Ward, Anne Dunckel, Emily Bernzott, Adam Wlostowski, Keith Sawicz, Caroline Kindall, Lindsay Kromel, Jenny Kissel, Riddhi Singh, Tim Gould, Tom Bassett, Erika Smull, Sara Sharkey, Austin Hopkins, Anne Brockett, Tom Bentley, Kerry Michael, and the Hydrogeophysics Field Camp participants (both in 2011 and 2012).

Additionally, I would not have been able to complete this work without support from a NSF Graduate Fellowship DGE-0750756, NSF Grant EAR-0911435, and a Penn State Graduate School University Graduate Fellowship.

Finally, I would like to thank my family for their unconditional love and support through every moment of my education. Bryan Kaproth, you've been my anchor and I can't tell you how much I appreciate our scientific discussions as well as all of the small things you've done to make these last few months a little easier.

Chapter 1

Introduction

Stream temperature is an important water quality parameter, particularly in headwater streams where smaller discharges can lead to highly dynamic thermal patterns (*Kim and Chapra, 1997)*. Sharp rapid increases in stream temperature can lead to negative impacts on fish, ranging from a temporary loss of equilibrium and motor activities to mortality (*Agersborg, 1930; Logue et al., 1995)*. In fish, a sudden change of only 2°C has been shown to cause unbalanced movement, while a sudden change of 4°C can cause oxygen deprivation (*Agersborg, 1930)*. Additionally, excess heat can affect the habitat and food supply of invertebrates in the stream (*Hogg et al., 1995*). Stream temperature also influences chemical and biological reactions that provide ecosystem services like nutrient uptake and transformation (*Kim and Chapra, 1997; Alexander et al., 2007)*. The ability of headwater streams to retain nutrients is crucial to the water quality of downstream environments (*Lowe and Likens, 2005)*. Many recent investigations into stream temperature are focused on seasonal or annual trends, particularly changes related to global climate change; impacts from storm events are more often disregarded (*Kaushal et al., 2010; Arismendi et al., 2012)*.

Previous studies in forested watersheds have observed storm events that on average slightly lower or cause negligible impacts on stream temperature (*Smith and Lavis, 1974; Shanley and Peters, 1988; Brown and Hannah, 2006*). A common explanation has been that precipitation infiltrates into the watershed's groundwater system, raising the water table. Near the stream, this water table rise creates a hydraulic gradient that drives the discharge of "older"

groundwater that is often cooler that pre-event stream temperature. This influx of cool groundwater lowers stream temperatures. For storms that occur in forested headwater systems, previous studies show that larger amounts of precipitation and higher precipitation intensities cause larger decreases in stream temperature (*Brown and Hannah, 2006*), suggesting that a greater groundwater contribution to streams occurs in response to larger precipitation intensities.

In contrast, in urban watersheds, stream temperature often increases during storm events due to impermeable surfaces that disconnect the groundwater system from the surface water system. The inability of precipitation to infiltrate into the near-surface aquifer increases the runoff amount, the rate that runoff reaches streams, and runoff temperature as it moves over paved surfaces heated by solar radiation (*Jones and Hunt, 2009; Natarajan and Davis, 2010; Jones and Hunt, 2010)*. For storms that occur in urban systems, we might expect that larger amounts of precipitation and higher precipitation intensities would cause larger increases in stream temperature.

This type of storm response observed in urban streams (rapid, large magnitude stream temperature increases) has not been reported in the literature for forested or headwater streams, but our recent observations suggest that it does occur. In a recent headwater stream field campaign in a primarily forested watershed, we observed that one-third of all monitored storms caused increases in stream temperature. Swift stream temperature changes of this magnitude may have unexpected potential negative impacts on the stream ecosystem.

Chapter 2

Study Site & Field Methods

2.1 Study Watershed Characteristics

The field site is located on an unnamed tributary to Shaver's Creek in Huntingdon County in central Pennsylvania (Figure 2-1), approximately 700 m from the Susquehanna Shale Hills Critical Zone Observatory (CZO) (*Jin et al., 2010*). The study reach is located primarily within what used to be the lakebed of the constructed Lake Perez reservoir. The upstream 1.5 km^2 catchment area is approximately 92% forested with less than 1% of the area covered by impervious surfaces (paved roads, gravel roads, structures) (*Homer et al., 2004*). The remaining portion of area is covered by meadow and lawn.

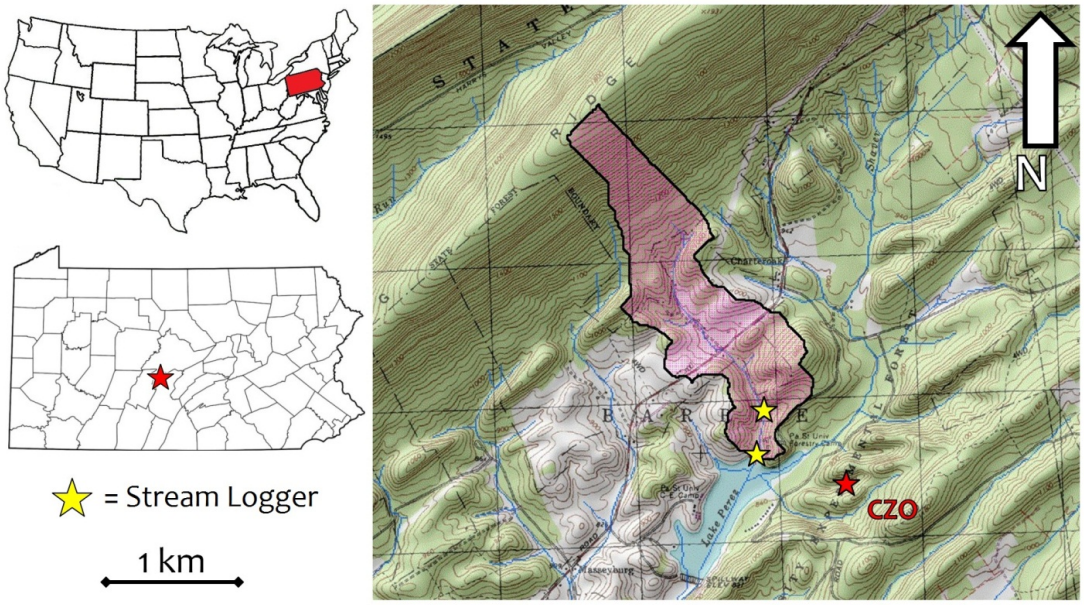

Figure **2-1**: Overview map of the study watershed boundaries (pink) and surrounding area (modified from *Stuckey and Hoffman, 2010*).

2.2 Basin Geology

The average depth to bedrock within the watershed is approximately 1 m (*Stuckey and Hoffman, 2010*). The northern border of the watershed is formed by Leading Ridge. The geologic units within the watershed are Silurian in age and include the following units: Bloomsburg and Mifflintown Formations (*Sbm*), Wills Creek Formation (*Swc*), Clinton Group (*Sc*), and Tuscarora Formation (*St*) (Figure 2-2)**.**

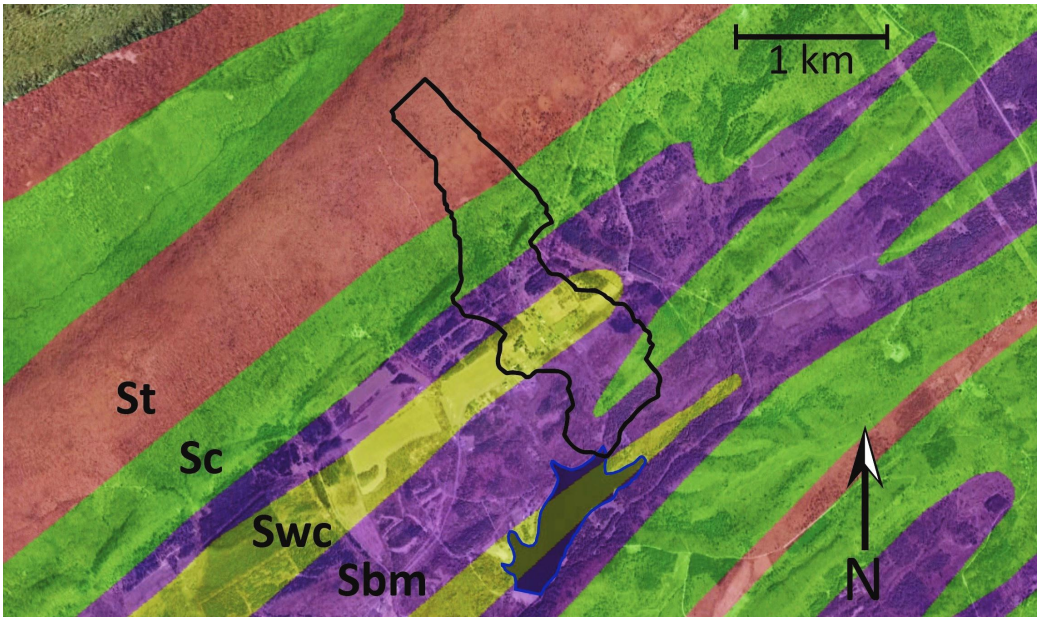

Figure **2-2**: Overview map of the geologic formations in the area surrounding the study watershed. The boundary of the watershed is shown with the heavy black line. Geologic map data provided by the U.S. Geological Survey (*Dicken et al., 2008*).

All four of these formations are fracture-dominated siliciclastic aquifers (*Fulton et al., 2005*). The Wills Creek Formation and the Bloomsburg and Mifflintown Formations are primarily shale, while the Tuscarora formation is a thick-bedded quartzitic sandstone and the Clinton group is composed of fossiliferous sandstone, hematitic sandstone, and shale (*Fulton et al., 2005*). For more detailed descriptions of these geologic units, see Doden and Gold (*2008*).

2.3 Regional Climate and Hydrologic Conditions

The watershed's drainage area is within the humid continental climate zone. This zone is characterized by seasonal extremes with humid, hot summers and cold winters. For mean monthly air temperature data collected in the region between 1899 and 2012 see Appendix A. The watershed is also within the Ridge and Valley Province of the Appalachian Mountains, which assists in creating greater air temperature extremes than are experienced in other areas of the state (*Pennsylvania State Climatologist, 2012*).

Climatologic data is available from the Shale Hills CZO meteorological station and includes air temperature, precipitation, relative humidity, wind speed, incoming solar radiation and barometric pressure data collected at sub-hour intervals. Precipitation is well distributed throughout the year (Appendix A). Mean precipitation for the region is 106 cm annually (data from 1899 to 2012) with maximum mean monthly precipitation falling in May and minimum mean monthly precipitation falling in February (*Pennsylvania State Climatologist, 2012*). Mean annual groundwater recharge in the watershed is estimated to be between 30 and 35 cm from data collected between 1971 and 2000 (*Reese and Riser, 2010*). Within the drainage area, the mean annual recharge as a percentage of precipitation is estimated to be between 30 and 35% (*Reese and Risser, 2010*). In the nearby Spring Creek watershed, evapotranspiration is estimated to be 43 cm annually, approximated from precipitation and long-term discharge data from 1968 to 2002 (*O'Driscoll and DeWalle, 2006*).

2.4 Field Methods

We have recorded stream stage, temperature, and fluid electrical conductivity every 15 minutes since April 1, 2011. The data used in these analyses extends from April through September of 2011. Stream temperature is recorded at two locations (Figure 2-1). The downstream location uses a HOBO U20-001-04 data logger recording stream temperature and stage. The second location is 200 meters upstream and uses a Solinst Diver Levelogger Model 3001 that records both stream temperature and fluid electrical conductivity. During the six months of record analyzed, mean daily stream temperature ranged from 5.7 ^{o}C on April 2, 2011 to 25.0 ^{o}C on July 22, 2011. Over the same six months of record, mean stream fluid electrical conductivity (EC) was 260 µS/cm, while the EC of groundwater sampled in shallow wells near the stream was often three to four times larger than the EC of the stream.

The change in stream temperature during a storm event is calculated as the difference between the stream temperature at the time of initial precipitation and the stream temperature at the time of maximum stream discharge in response to the storm.

Given the difficulty of directly measuring precipitation temperature, wet bulb temperature is used as an acceptable approximation of precipitation temperature (*Kim and Chapra, 1997*). Wet bulb temperature indicates the amount of moisture in the air and is the lowest temperature that can be reached by evaporation only. When relative humidity is near 100%, precipitation temperature (as estimated by wet bulb temperature) approximates air temperature. We use the empirical "inverse" relationship provided in Stull (*2011*) to calculate wet bulb temperature from measurements of relative humidity and air temperature (Equation B-1 in Appendix B). When used within the equation's constraints (constant barometric pressure, temperature between -20 °C and 50 °C, and relative humidity between 5% and 99%) the

empirical solution solves for wet-bulb temperature within ±1°C (*Stull, 2011*). The additional error generated when this empirical solution is used with a non-constant pressure is small, particularly in regions like central Pennsylvania where the relative humidity is primarily above 50% (see Figure B-1 in Appendix B for error generated).

2.5 Estimating Discharge from a Stream Stage Record

At this field site, it was necessary to estimate a discharge record from a stream stage record. Without a direct record of discharge or a stage-discharge rating curve, we were forced to estimate discharge using Manning's equation and other estimated stream parameters (see appendix C for a detailed explanation) (Figure 2-3).

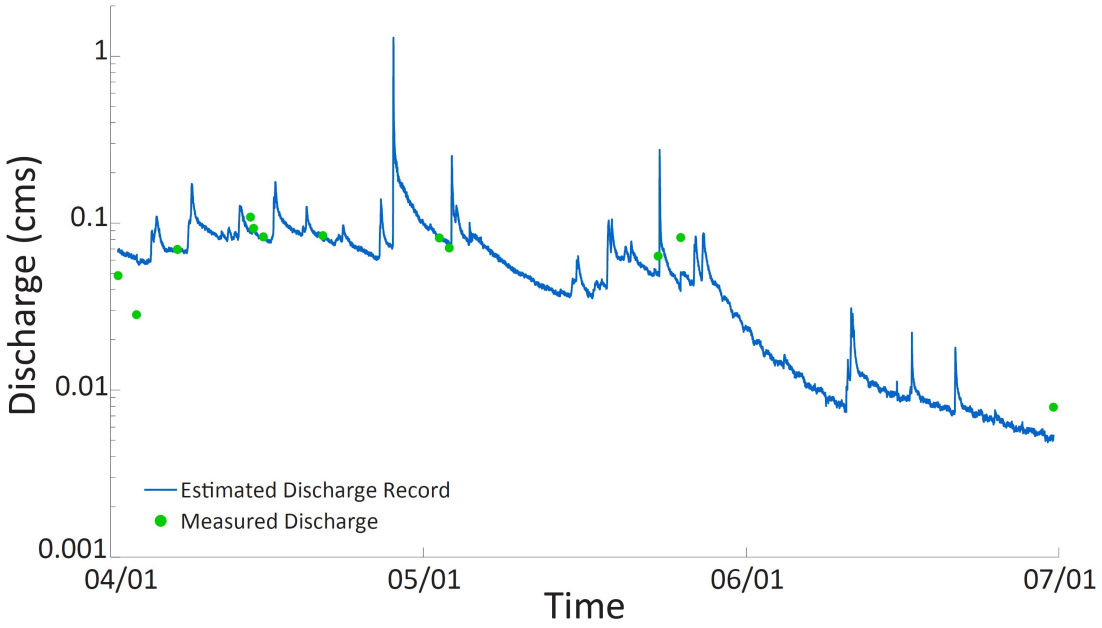

Figure **2-3**: Semi-log plot of the manually observed discharge measurements as the green points and the estimated discharge record as the blue line over 3 months of record.

Estimates of flow range between 0.007 cms in mid-June to 1.29 cms during a large storm at the end of April. As we only had stage measurements at one point along the stream, we also used a hydrodynamic flow routing model to determine how storm pulses would move through the length of the stream. To solve for discharge along the stream reach through time, we used St. Venant's Equation, coupled with conservation of mass, to numerically solve for the temporal and spatial evolution of the system. Manning's Equation was used again to describe the friction force in the St. Venant's Equation. For a detailed report on this flow routing module, see appendix D.

When describing 1D, vertically integrated, unsteady, non-uniform flow, St. Venant's equation can be written as:

$$\frac{\partial \mathrm{Q}}{\partial \mathrm{t}} + \frac{\partial \mathrm{QV}}{\partial \mathrm{x}} + \mathrm{gA}\left(\frac{\partial h}{\partial x} + S_o + \mathrm{S_f}\right) = 0 \qquad \text{Eqn. 2-1}$$

where Q is stream discharge (cms), v is water velocity (m/s), A is the cross-sectional area of the channel (m^2), h is the cross-sectional average water height (m), S_o is the channel bottom slope, S_f is the friction slope and is derived from Manning's equation, x is space along the channel length (m), and t is time (sec). From left to right, the terms of the equation include local acceleration, advective acceleration, pressure force, gravity force, and the friction force terms. This equation can be simplified into a few different forms depending on how many terms of the equation are included. The dynamic wave equation includes all of the terms shown above. The diffusion wave equation neglects both acceleration terms. The kinematic wave equation neglects all of the terms but the gravitational and friction force terms.

Though this may seem simple, the kinematic wave equation does a good job of flow routing when the system does not include tides, tributary inflows, or reservoir operations (*Chow et al., 1988*). It is also recommended that the bed slope of the channel be greater than 0.001

(the mean bed slope of this stream channel is 0.009). The kinematic wave equation assumes that the friction force is balanced by the gravitational force. The simplified form of the kinematic wave equation is:

$$\frac{\partial Q}{\partial x} + \alpha\beta Q^{\beta-1}\frac{\partial Q}{\partial t} = 0 \qquad \text{Eqn. 2-2}$$

where $\alpha = \left[\frac{nP^{2/3}}{\sqrt{S_o}}\right]^{0.6}$ and $\beta = 0.6$

For a large storm that occurred on May 23, 2011, the peak discharge 1000 meters downstream of the boundary condition occurred 22 minutes after the peak discharge at the boundary condition. The mean velocity of this kinematic flood wave in this system is 2.8 kilometers per hour or 0.8 meters per second. Over 1000 meters, the peak flow attenuates by 0.0005 cms or 0.2%. This is such a small attenuation that we make the assumption in our storm event analyses that there is no dispersion of storm flood waves through space or time in the reach (i.e. the flood wave "marches" down the reach without changing).

Chapter 3

Field Observations

Data from the two storms that caused the largest spikes in stream temperature are shown in Figures 3-1 and 3-2 with two days of background data prior to the storm and one day of data post-storm. On April 26th, 18.9 mm of precipitation fell while on April 28th, a total of 35.8 mm of precipitation fell with an average intensity of 9.8 mm/hr (Figure 3-1). The storm event caused a 3.5 °C increase in stream temperature above the pre-storm mean temperature of 12.8 °C. Stream stage rose from 0.27 m to a peak of 0.83 m and fluid electrical conductivity dropped from 200 µS/cm to 140µS/cm during the storm.

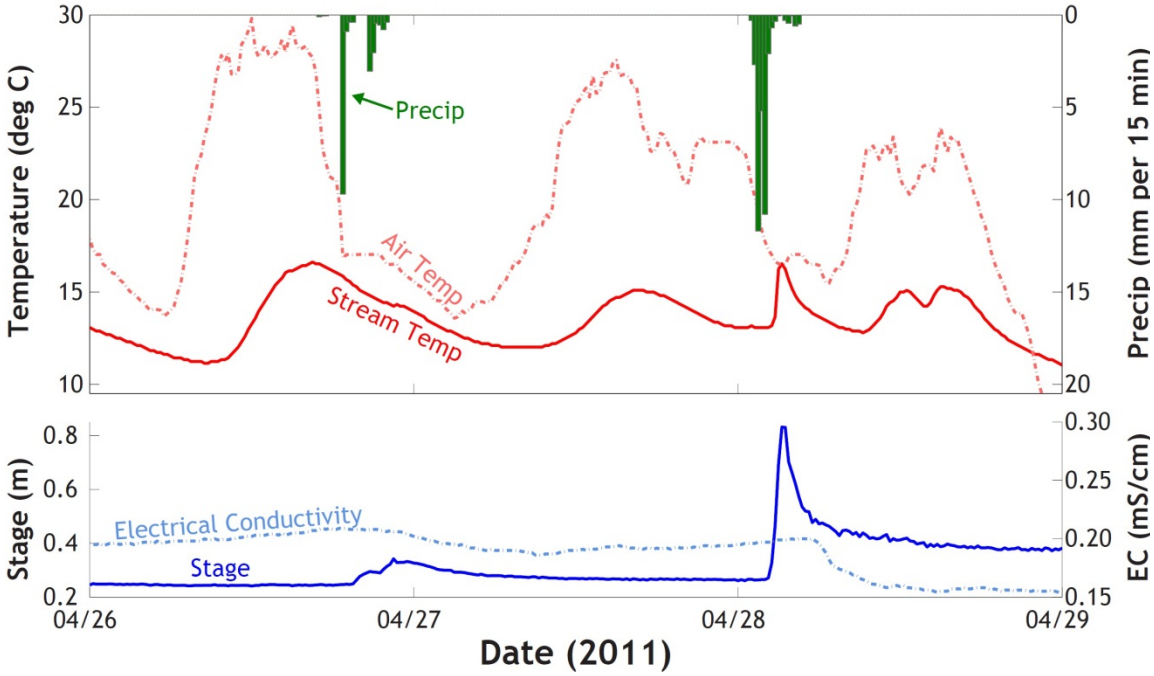

Figure **3-1**: Summary data collected during April 28th storm event including stream stage, stream temperature (from the downstream logger), fluid electrical conductivity, precipitation and air temperature.

While the previous storm on April 28th occurred in the middle of the night (when solar radiation was not contributing to stream temperature), this storm on May 23rd occurred in the middle of the afternoon (Figure 3-2). Despite this difference, we see similar behavior. On May 23rd, there was a total of 29.9 mm of precipitation at an average intensity of 36 mm/hr. The storm event caused a 3.8 °C increase in stream temperature above the pre-storm mean temperature of 13.7 °C. Stream stage rose from 0.27 m to a peak of 0.63 m and fluid electrical conductivity dropped from 230 µS/cm to 170µS/cm during the storm.

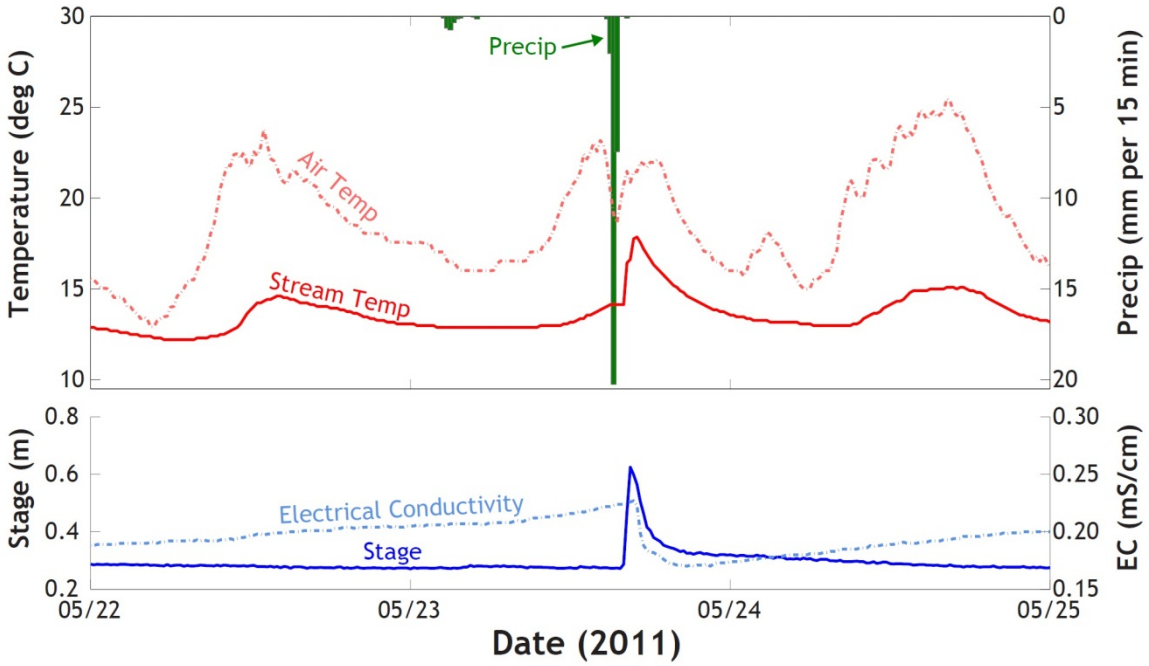

Figure **3-2**: Summary data collected during May 23rd storm event including stream stage, stream temperature (from the downstream logger), fluid electrical conductivity, precipitation and air temperature.

Beyond individual storms, we also present the observed changes in stream temperature for 87 storms observed over a six month period in 2011 (Figure 3-3). No storms were analyzed that produced less than 1 mm of precipitation. The stream temperature change during each storm was analyzed as the change from the temperature at the start of the precipitation to the

temperature at the time of peak stream stage. The average storm intensity was determined as the total amount of precipitation from a storm (mm) over the full duration of the storm (hr). One third of the storms that cause positive shifts in water temperature were increases in temperature larger than 0.5 °C. This third caused rapid stream temperature spikes (of up to 3.8 °C increase in less than 1 hour). See Appendix E for a table summarizing all storm data including date of storm, total storm precipitation, mean intensity, storm duration, and change in stream temperature associated with each storm.

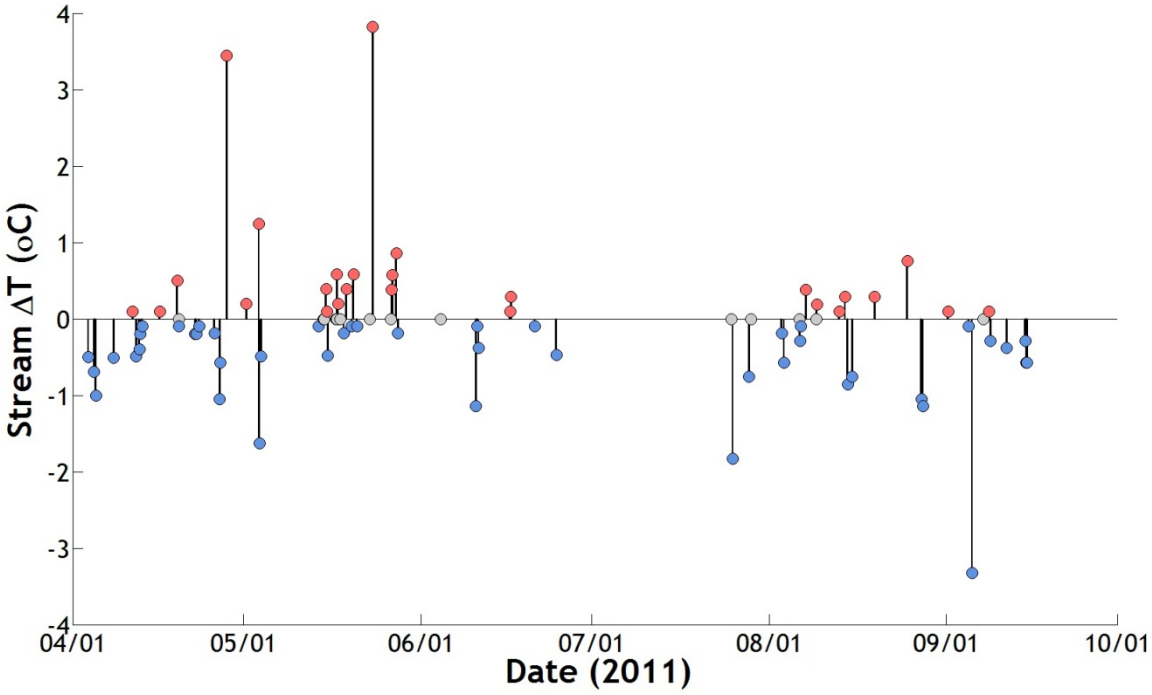

Figure **3-3**: Summary data of the 87 storms analyzed. Pink dots indicate an increase in stream temperature, blue dots indicate a decrease in stream temperature, and gray dots show no stream temperature change during a storm.

Not all storms cause increases in stream temperature (Figure 3-3). Still, nearly half of all storms cause either increases or neutral changes in stream temperature.

Chapter 4

Discussion of Physical Mechanisms

4.1 Expected Mechanisms for Storm Event Response

We examine the possible physical mechanisms that produce the observed discharge and unanticipated stream temperature responses to storms using the May 23, 2011 storm as a case-study (3.8 ^{o}C stream temperature increase in response to 30 mm of precipitation) for all of the analyses to follow in this chapter (Figure 3-2). We hypothesize that the primary driver of the observed discharge and stream temperature responses in the stream could be one of the following four physical mechanisms:

(1) Channel Interception: Warm precipitation falling directly on the stream channel causes the observed temperature spike.
(2) Channelized Runoff on Charter Oak Road: The one road that crosses the drainage area acts as an urban conduit. This conduit carries runoff to the stream very quickly over an impervious hot surface (potentially increasing runoff temperature).
(3) Overland Runoff: The storm is too intense for any significant infiltration of precipitation, therefore all effective precipitation on the 1.5 km^2 drainage area goes to runoff and causes the observed temperature anomaly.
(4) Subsurface Input: Precipitation is able to infiltrate as expected in a forested headwater stream, therefore warm lateral inflow to the stream is the primary mechanism behind the temperature anomaly.

For "worst-case" end-member hypothesis testing, we assume that each of these four mechanisms happens without impacts from any other mechanisms (e.g., all of the water that reaches the stream is solely from overland runoff). We also assume that the precipitation

measurements that were collected at the Susquehanna Shale Hills CZO (less than 1 kilometer away) are accurate and representative of the precipitation received within the study watershed. Finally, we assume precipitation amount and timing is spatially uniform across the entire 1.5 km^2 drainage area.

Before we test each proposed driver of stream response to the storm, we study which hydraulic mechanisms we would expect to control this event response. Direct channel precipitation occurs in all storms and can be expected in this system as well. Although the channel surface area is small (less than 1% of the drainage area), all precipitation that falls on the stream immediately becomes runoff. Surface runoff can include Hortonian overland flow where the hillslope is saturated from above and saturation overland flow where the hillslope is saturated from below. Subsurface event flow in the saturated zone can include flow from perched saturated zones or flow from local groundwater mounds, while subsurface event flow in the unsaturated zone can include matrix/Darcian flow and macropore flow. Appendix F contains information on what types of soil, geology, topographic, vegetative and water-input condition favor the various mechanisms for surface runoff and saturated zone subsurface flow (*Dingman, 2008*).

4.2 Stream Channel Interception

We are able to reject one hypothesized mechanism: direct precipitation onto the stream channel (without considering additional impacts from overland runoff or subsurface inflow) is not the controlling mechanism behind the discharge or stream temperature response observed. There are three lines of evidence for this conclusion.

First, if the temperature anomaly was caused solely by direct precipitation (falling at a warm temperature) on the stream, we would expect the stream temperature spike to coincide with the storm event since the mixing of the hot direct precipitation would be almost immediate into the streamflow. Instead we see that it takes more than an hour for discharge at our gauging station to peak and another half hour beyond that for the stream temperature spike to peak. Stream temperature does not even begin to rise until 30 minutes after precipitation has ceased.

Also, using a Lagrangian perspective to "follow" a parcel of stream water along the reach, we define the volume of this water parcel as being the cross-sectional area of the stream (estimated as 0.18 m^2 at the stage logger) prior to the storm multiplied by an arbitrary one-meter length, such that the initial volume of this parcel is 0.18 m^3. If direct precipitation controlled the anomalous temperature response, we would expect that the 30 mm of storm precipitation falling directly onto this parcel of water would account for the peak observed discharge. The volume of precipitation added to the parcel through the entire storm (30 mm depth) is 0.035 m^3. Therefore if direct precipitation on the stream accounted for signal, the predicted peak volume of this stream parcel would be 0.215 m^3. Instead, the observed peak volume is 811 m^3. The volume of direct precipitation on the stream channel can only account for approximately 5% of the increase in this stream parcel's volume due to the storm.

Finally, continuing with this Lagrangian perspective and the known volume of the water parcel, we also know that the pre-storm stream temperature was 13.7 °C and that the peak stream temperature during the anomaly was 17.5 °C. Using a simple end-member mixing analysis (Equation 4-1) and assuming that the 30 mm of precipitation entered the parcel as an instantaneous pulse of water, we determine that the direct channel precipitation would need to

be 38 °C to create the observed stream temperature spike if it were the sole controlling mechanism on stream temperature response to the storm.

$$T_{contribution} = \frac{(V \cdot T)_{stream\ peak\ storm\ flow} - (V \cdot T)_{stream\ background}}{V_{contribution}} \qquad \text{Eqn. 4-1}$$

In equation 4-1 above, *T* is temperature and *V* is volume. The subscripts are as follow: *contribution* refers to the temperature and volume of the input being analyzed (in this case direct precipitation on the stream), *stream background* refers to the temperature (13.7 ºC) and volume of the stream parcel before the storm, and *stream peak storm flow* refers to the peak temperature (17.5º C) and peak volume observed for that stream parcel. Our estimation of the actual precipitation temperature is 18.3 ± 0.7 °C during the storm (approximated by empirical estimations of wet bulb temperature using air temperature and relative humidity data), which is notably less than the required 38 ºC.

4.3 Runoff from Precipitation on Charter Oak Road

There is one paved road that runs perpendicular to the stream through the drainage area of this stream. We seek to test whether this road could act as a conduit to carry both heat and water quickly to the stream. We simplify the problem by assuming that the road is rectangular with dimensions of 775 meters by 6 meters wide. We also assume that the fraction of road on each side of the stream are approximately equal and have similar slopes (approximately 6%) towards the stream channel. With these dimensions, the road has an impervious surface area of approximately 4,650 m^2. Using Figure H-1 in Appendix G, we determine that an estimate of sheet flow velocity over this road at a 6% slope is 1.5 m/s.

We also know from the kinematic flow routing model that the stream flow is moving at an estimated 0.8 m/s during the peak storm response. To simplify, we round this velocity to 1 m/s. Again we use a Lagrangian perspective and an end-member analysis (using equation 4-1) to investigate the contribution of water from the road to a stream parcel with a volume equal to the cross-sectional area of the stream prior to the storm multiplied by an arbitrary one-meter length. As the road is 6 meters wide, we make the simplifying assumption that a parcel of water that is one meter long (moving at 1 m/s) will receive contributions from the road for approximately 6 seconds. Within these 6 seconds, the surface area of road that will contribute to that parcel is 18 m^2 (9 m^2 of road on each side of the stream with this runoff moving at 1.5 m/s). In the worst case scenario, we assume that the 30 mm of rain fell nearly instantaneously and within the 6 seconds, this depth of water over the 18 m^2 of contributing road area will enter the stream. This is an input of 0.54 m^3 to our parcel of water that had a background volume of 0.18 m^3, which would now have a predicted total peak volume of 0.72 m^3. In actuality, the peak total volume of this parcel is only slightly larger at 0.81 m^3.

With these volume estimates, if the road were the only contributing source of water, the runoff from the road would need to be at 18.8 ºC to create the increase in temperature that we observed. This temperature is only 0.5ºC higher than the estimated precipitation temperature during the storm and is within the error of that estimate (wet bulb temperature during the storm is estimated to be 18.3 ± 0.7 °C).

However as a part of this worst-case scenario hypothesis testing, we have estimated the largest possible amount of runoff that could enter the parcel of water being analyzed while passing by the road. In reality, the 30 mm of rain did not fall instantaneously and the entire depth of rain would not contribute to the particular water parcel of interest. At the storm's most

intense time, 20 mm of rain fell within 15 minutes. This would produce a depth of 0.13 mm of precipitation in 6 seconds, which would only be a volume contribution of 0.002 m^3. With such a small volume contribution, the temperature of that runoff would need to be 325 ^oC. This is an impossibly high temperature for the road runoff.

Therefore, from the worst case scenario analysis alone we are unable to reject the road as a possible driver of the observed stream temperature anomaly. However, if we consider a more reasonable volume of contribution (taking into account actual rainfall rates), it becomes more unlikely that the road was the sole driver of this temperature anomaly.

4.4 Surface Runoff to the Stream

Woodruff and Hewlett (*1970*) predicted that 8% or less of precipitation that falls on watersheds in central Pennsylvania would become a part of that stream's event-flow (Q_{ef}, identifiable stream flow response to a storm). The remainder of precipitation goes to evapotranspiration, groundwater outflow, or to stream flow at a much later time (beyond the time of defined event response) (*Dingman, 2008*). For the May 23, 2011 storm, precipitation measurements show that 30 mm of rain fell in 1 hour. With a drainage area of 1.5 square kilometers, this storm produced an estimated 45,000 m^3 of water within the watershed. Some of this water infiltrates into the subsurface, some becomes overland runoff, and some goes to evapotranspiration. The portion of water that quickly reaches the stream (as opposed to days or weeks after the storm event) is called event flow.

We use baseflow separation to determine what volume of water in the stream's discharge record is event flow, Q_{ef}. Using the concave method (*Linsley and Kohler, 1951*) of

hydrograph separation, we calculate that only 2,200 m^3 of storm flow reached the stream (Figure 4-1). This is 5% of the total precipitation that fell on the drainage basin. This 5% event flow is equivalent to the fraction of effective rainfall and can be translated into a depth of effective rainfall, or water input, (W_{eff}) by dividing Q_{ef} by the watershed area. For this method of baseflow separation, W_{eff} would equal 1.5 mm.

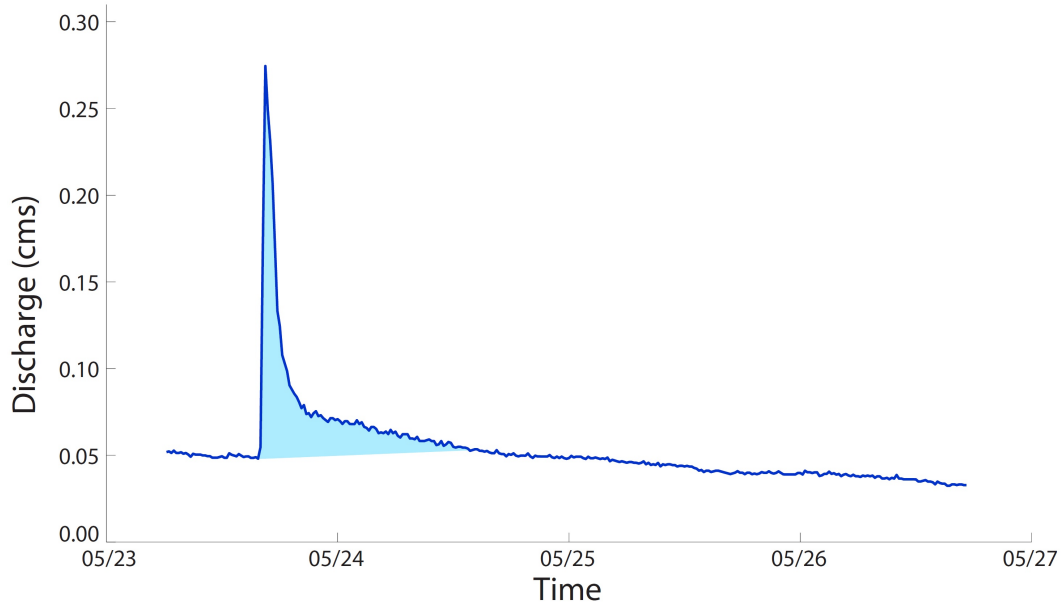

Figure **4-1**: Separation of baseflow from event-flow (shaded light blue) for the May 23, 2011 storm event. The volume of the event-flow is approximately 2,200 m^3.

Another way to compute W_{eff} is the NRCS SCS Curve-number method, which is commonly used to predict the amount of direct runoff from rainfall events in small watersheds in rural areas (*Dingman, 2005*). This method was developed from empirical analysis of runoff from USDA monitored catchments. The approach takes into account land cover types, antecedent moisture conditions, and hydrologic soil groups within the watershed. These hydrologic soil groups are defined and mapped by the NRCS and range from the most permeable soils in group A (sands, loess, etc.) to the least permeable soils in group D (heavy clays). Table 4-1 below presents the required data to compute W_{eff} for this study watershed.

Land cover type and area are estimated from Homer et al. (*2004*), while the hydrologic soil groups are mapped by the U.S. Natural Resources Conservation Service (*2012*).

Table **4-1**: Watershed data required to determine the watershed weighted-average curve number including land cover type, hydrologic soil group, area of land cover type, percent of total area, and curve number for type of land cover.

Land Cover Type	Hydrologic Group	Area (km^2)	% of Total Area	Curve #
Forest, Fair Condition	D	0.15	10%	82
Forest, Fair Condition	C	0.825	55%	76
Forest, Fair Condition	B	0.405	27%	65
Paved Road, Open Ditch	C	0.00675	0.45%	92
Gravel Road	C	0.00825	0.55%	89
Farmstead	C	0.09	6%	82
Urban Lawn, Good Condition	C	0.015	1%	74
Watershed Weighted-Average CN	-	*1.5*	*100%*	*74.1*

The weighted-average curve-number (assuming average antecedent soil moisture conditions) is 74.1. Equation 4-2 is used to determine W_{eff} where *CN* is the watershed weight-averaged curve-number and *W* is the total 30 mm of rainfall (Dingman, 2008).

$$W_{eff} = \frac{\left(W - \left[0.2 \cdot \left(\frac{1000}{CN} - 10\right)\right]\right)^2}{W + \left[0.8 \cdot \left(\frac{1000}{CN} - 10\right)\right]} \qquad \text{Eqn. 4-2}$$

With $W = 30\ mm$ and $CN = 74.1$, W_{eff} is 0.06 inches or 1.5 mm. This is equal to the value of W_{eff} estimated with the concave method of baseflow separation: 5% or less of the precipitation that falls on the entire drainage area became part of the event response in the stream (through surface runoff or subsurface flow).

We now complete an end-member analysis (using equation 4-1) of overland runoff using 1.5 mm as the effective depth of rain over the watershed, assuming that no other physical mechanisms transport this depth of precipitation. The mean basin slope is 10° or 17% (*Stuckey and Hoffman, 2010*). Assuming that this overland runoff is moving primarily through forest with

heavy ground litter (the watershed is 92% forested), we use Appendix G to determine that an estimate of this overland flow's velocity is 0.25 m/s.

Continuing with the Lagrangian perspective of a parcel of water moving along the stream reach, we consider what volume of water from overland runoff would contribute to the stream parcel over its 1.5 km length. Again, the parcel's volume is equal to the cross-sectional area of the stream prior to the storm multiplied by an arbitrary one-meter length. We assume that the 1.5 mm depth of effective rainfall occurs instantaneously over the watershed and then begins moving at 0.25 m/s towards the stream (without infiltrating or evaporating). Rounding the estimated stream velocity from 0.8 m/s to 1 m/s (for simplicity), the parcel of stream water would take approximately 25 minutes to move the 1.5 kilometers from the top of the reach to the point at which we monitor stream temperature. In this 30 minutes, contributions to the stream will come from 750 m^2 of the watershed (375 m^2 on each side of the stream). With a depth of 1.5 mm and an area of 750 m^2, the volume contribution to the stream parcel is 1.125 m^3 with a total peak volume of 1.3 m^3. This is significantly larger than our estimate of the peak total volume at 0.81 m^3. With this volume of runoff contributing to the stream, the runoff would only need to be 18.1 ^oC to create the observed spike in stream temperature.

This calculation suggests that overland runoff could be the primary mechanism of the observed stream response. With only 5% of the precipitation becoming runoff to the stream, this is more than enough water input to the stream to explain the increase in discharge. In reality, we would expect less runoff than we have estimated here to reach the stream for two reasons: (1) the entire 1.5 mm depth of effective precipitation did not actually fall instantaneously on the watershed, and (2) precipitation that fell further away from the stream

has more opportunities through time and space to evaporate and infiltrate before reaching the stream as overland runoff.

4.5 Subsurface Storm Flow to the Stream

Infiltration is required before subsurface storm event flow can begin to contribute to the stream. To test whether infiltration could be the primary response mechanism in the watershed, we look at the hydrologic properties of the soil units within the region of the watershed shown in Figure 4-2.

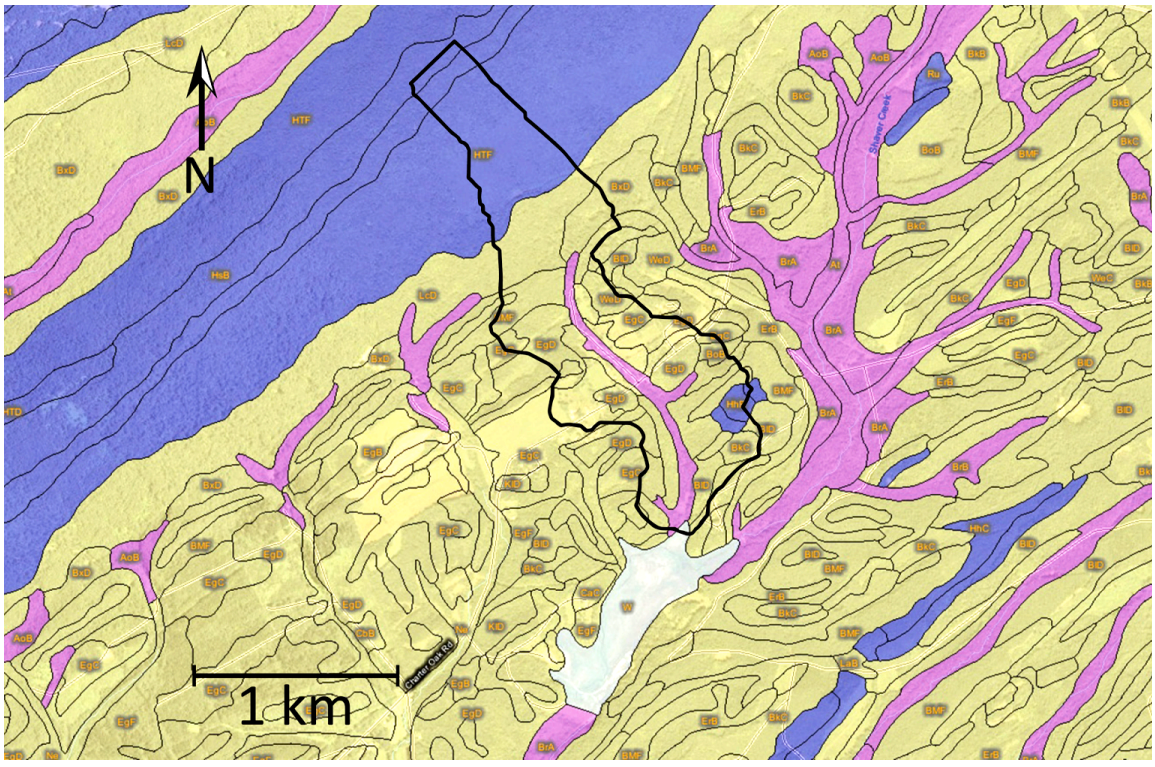

Figure **4-2**: Map of hydrologic soil groups near the watershed drainage area (watershed boundary shown with heavy black line). Blue soils are hydrologic group B, yellow soils are hydrologic group C, and pink soils are hydrologic group D. Map modified from the *Web Soil Survey* created by the U.S. Natural Resources Conservation Service (*2012*).

Almost all of the soils within the watershed boundary are of hydrologic groups B and C (Table 4-1). The soils directly surrounding the small stream are Brinkerton soil loam, which is part of the D hydrologic soil group (the least permeable group). Soils within hydrologic unit D are subject to high overland-flow potential with a very low minimum infiltration capacity when thoroughly wetted (less than 1.3 mm per hour). Soils further from the stream are primarily a mix of C and D hydrologic soil groups. Similar to group D, group C soils also have a low minimum infiltration capacity when thoroughly wetted (1.3 mm to 3.8 mm per hour). At the watershed edge bounded by Leading Ridge, there are a few soil units that are part of the hydrologic soil group B. These soils are more permeable and can handle infiltration rates of 3.8 to 7.6 mm per hour.

This analysis of the soil groups present within the watershed show that regardless of the time of year, precipitation falling on this drainage area will have a difficult time infiltrating into these low permeability soils, particularly during intense storm events where more than 5 to 10 mm fell within an hour. During this storm, 20 of the 30 mm of precipitation fell within 15 minutes. With such a high storm intensity during that time, we can be relatively certain that overland runoff occurred. We also know that overland flow is a faster transport mechanism than subsurface flow (*Dingman, 2008*). Finally, overland flow has shown to be a primary mechanism in the rising limb and peak discharge of a storm hydrograph (*Mays, 2005*). For these reasons, we conclude that while sub-surface flow may have been a contributor to the stream response at later times, we can reject sub-surface flow as the primary mechanism behind the peak discharge and peak temperature anomaly in the stream.

4.6 Summary of Contributing Mechanisms

From these analyses we can make the following conclusions:

(1) We reject channel interception as the primary mechanism behind the stream's storm response.

(2) We were unable to reject runoff from the road as the mechanism behind the anomalous temperature response in the stream; however, it is an unlikely mechanism unless the full 30 mm of rain that fell on the road contributed to the stream instantaneously and simultaneously.

(3) Two methods of hydrograph separation each predict that less than 5% of the total precipitation that fell on May 23, 2011 made it into the stream during the time defined as event-response.

(4) The soils in the drainage area have a very low permeability and are prone to causing overland flow, particularly during intense storm events like the storm on May 23, 2011. Therefore, we reject subsurface flow to the stream as the primary cause of event response in the stream.

(5) With a lag-to-peak flow time of 2 hours and a drainage basin area of 1.5 km^2, it is much more likely that overland flow was a primary mechanism rather than subsurface storm flow (*Kirkby, 1988*).

One mechanism that was not strongly considered, but may deserve more attention is flow through bedrock fractures. As stated earlier, the bedrock formations lying within this drainage area act as fracture-dominated siliciclastic aquifers. Bedrock fractures may be a viable flow mechanism in contributing to the event response, particularly in areas where the soil layer

is thin and bedrock is exposed. Also, the soil in the headlands of the watershed is more permeable (part of hydrologic soup group B) than soils further down the watershed. It is possible that in the headlands of the watershed, the bedrock is closer to the surface with thinner, more permeable soil above it. This would allow for an increased amount of the rainfall to reach subsurface fractures. Unfortunately, it is difficult to estimate what percentage of precipitation enters these bedrock factures and what percentage of flow within the fractures reaches the stream within the time of storm event response.

4.7 An Alternative Model for this Headwater Stream

As stated previously, if the water entering the stream in response to the storm were "older" groundwater input as expected for a forested headwater stream, we would anticipate a stream temperature decrease as groundwater temperatures are often cooler than pre-storm stream temperatures. Regardless of the physical mechanism, we conclude that the stream event-flow is composed of "new" water: precipitation and runoff at warm temperatures. We determine that this is viable by using an end-member mixing analysis to determine what temperature the storm event-flow would need to be to raise the stream's background temperature of 13.7^{o}C to the peak observed temperature of 17.5 ^{o}C. Prior to the storm, we estimate that the stream's discharge was 0.05 cms. Peak discharge in response to the storm was 0.30 cms. We make the simplifying assumption that to increase the stream discharge from the background flow rate of 0.05 cms to the peak flow of 0.30 cms, 0.25 cms of storm flow are added at a uniform constant temperature. We use equation 4-3 below to determine what

temperature the 0.25 cms ($Q_{storm\ flow}$) event discharge would need to be at to raise the stream temperature the observed 3.8 ºC.

$$T_{stormflow} = \frac{(Q \cdot T)_{total\ peak\ flow} - (Q \cdot T)_{background}}{Q_{stormflow}} \quad \text{Eqn. 4-3}$$

This end-member analysis suggests that the water input would need to be at 18.3 °C if 0.25 cms were added to the background 0.05 cms. If we hypothesize that all of the water being added to the stream is "new" water from rainfall (not groundwater), our best estimate of the real temperature of the "new" water is to use wet-bulb temperature as an approximation of precipitation temperature (see Appendix B). The mean wet-bulb temperature for one hour before the storm event and for during the one hour of precipitation was 18.3 ºC.

While this match between our estimated wet-bulb temperature and the temperature required to raise the stream temperature with the known increase in discharge is compelling, the wet-bulb temperature is an approximation and does have some error associated with it. Therefore we do a simple sensitivity analysis to determine how the volume of predicted storm flow would change if the temperature of the storm flow were different (Table 4-2).

Table **4-2**: Sensitivity analysis of how changes in the estimated storm-flow temperature (wet-bulb temperature) affect the required volume of storm-flow to produce the observed stream temperature change.

Estimated Temperature of Storm-flow* (ºC)	Required Volume of Storm-Flow (cms)	Total Peak Flow ($Q_{background}$ + $Q_{storm\ flow}$)
17.7	0.95	1.00
17.9	0.48	0.53
18.1	0.32	0.37
18.3	**0.25**	**0.30**
18.5	0.19	0.24
18.7	0.16	0.21
18.9	0.14	0.19

** Temperature of storm-flow approximated by wet-bulb temperature as an estimate of precipitation temperature*

As shown in Table 4-2, small changes in the wet-bulb temperature create big impacts on the required volume of storm-flow to create the observed change in stream temperature. However, even with this high sensitivity, this calculation and analysis show that if the precipitation temperature were near 18.3 ^{o}C, the temperature of the precipitation alone would be enough to explain how the increase in stream discharge (with "new" water input at 18.3 ^{o}C) produced a 3.8 ^{o}C increase in stream temperature in response to the storm.

This conclusion that the stream's storm response is composed of "new" water instead of displaced "old" groundwater is supported by the changes in stream fluid electrical conductivity (Figures 3-1 and 3-2). The observed stream temperature "spikes" are accompanied by strong decreases in stream fluid electrical conductivity (EC). This suggests that the storm discharge carrying the anomalous temperature signal is fresher than the pre-storm background stream EC. As groundwater EC values in the drainage area are three and four times the background EC values of the stream, it is probable that most of the water entering the stream during peak storm-flow is not stored groundwater, and is instead precipitation (either direct or overland run-off). This finding supports our conclusion that a new system understanding may be appropriate: the observed response in this forested headwater stream is primarily composed of "new" (warmer, lower EC) water rather than the predicted "older" (cooler, higher EC) groundwater.

Chapter 5

Discussion of Response Seasonality

5.1 Seasonality of Stream Temperature Response to Storms

There is a relationship between time of year and large stream temperature changes during storms (Figure 3-3). Storms that cause strong increases in stream temperature occur primarily in the spring months (April through June). Storms that cause strong decreases in stream temperature occur primarily in the fall months (July through September). The mean change in stream temperature in the spring months is 0.04 °C, while the mean change in stream temperature in the fall months is – 0.35 °C. A two-sample t-test assuming unequal variances was completed to determine if this difference between the spring stream response to storms is significantly different from the stream response to storms in the fall. With a two-tail *p*-value of 0.033, this difference is statistically significant (Appendix H).

To consider what type of storm we would expect to cause these stream temperature responses, we examine the relationship between stream temperature change for every storm and either the corresponding mean storm intensity or total storm precipitation (Figures 5-1 and 5-2). The zones of color in these figures show the conceptual model of what we might expect to occur in an urban environment (pink zone) and in a forested watershed (green zone).

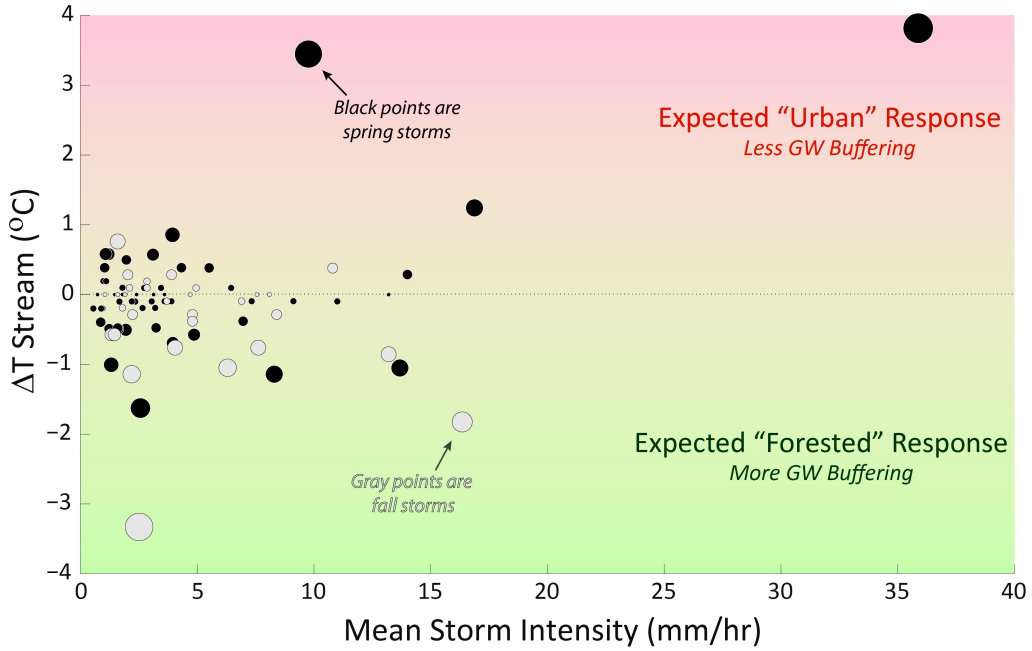

Figure **5-1**: Mean storm intensity (mm/hr) versus change in stream temperature for all storms observed. Black dots are storms that occurred in the spring months (April through June), while gray dots are storms that occurred in the fall months (July through September). The size of the dot is a secondary way of showing the size of the stream temperature change.

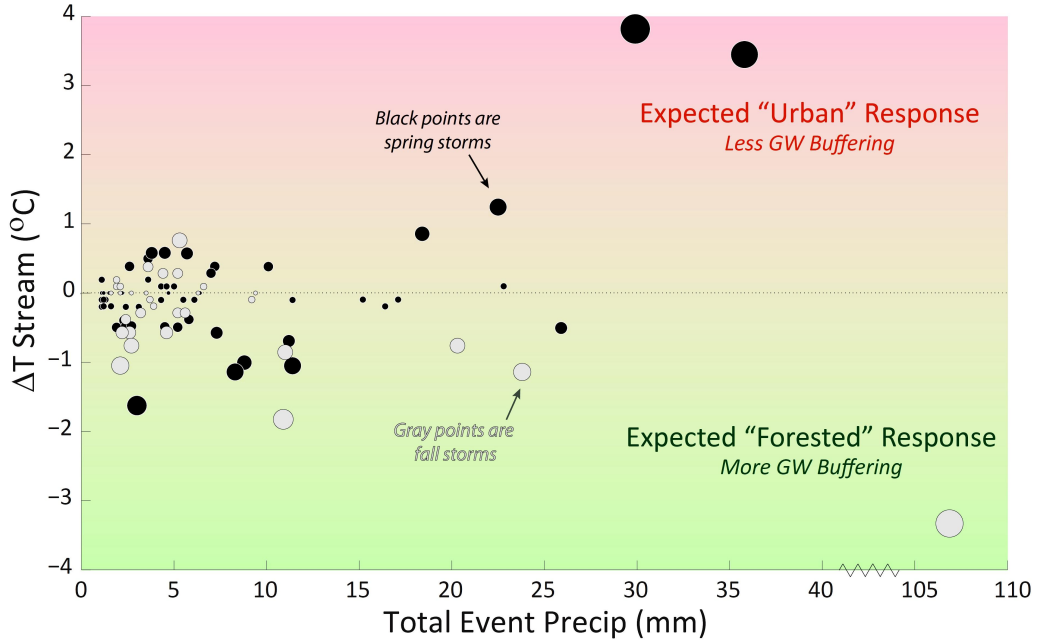

Figure **5-2**: Total event precipitation (mm) versus change in stream temperature for all storms observed. Black dots are storms that occurred in the spring months (April through June), while gray dots are storms that occurred in the fall months (July through September). The size of the dot is a secondary way of showing the size of the stream temperature change.

In this forested headwater stream, there are storm events with stream temperature changes that plot as expected (those below the dotted line, in the green zone), but there are also storm events that plot like urban stream temperature responses (those above the dotted line, in the pink zone). The largest storms and most intense storms cause the strongest changes in stream temperature (both positive and negative). Also, the storms that caused the largest increases in stream temperature tend to be the largest and most intense storms of the spring months, while the storms that caused the largest decreases in stream temperature tend to be the largest and most intense storms of the fall months. In contrast to our observations, a previous study found that stream temperature increases during storms were associated with short, small, low-intensity storm events and represented smaller relative departures from pre-event temperatures (*Brown and Hannah, 2006*).

These results suggest that there may be an alternative to the current understanding that storm events cause decreases in temperature in forested headwater streams that are proportional to the storm size and intensity. Instead, as mentioned previously, we conclude that much of the observed stream response is "new" water instead of the expected displacement of "old" groundwater to the stream. In particular, the limited connection between the groundwater system and the stream may allow the seasonably variable climate (precipitation temperature, air temperature, relative humidity) to more greatly control stream temperature response to storms. Similarly, a previous study in an urban environment has shown that the amount of groundwater connection and buffering is strongly inversely related to how many "hot flashes" occur in the study stream during storms (*Nelson and Palmer, 2007*).

5.2 Seasonality of the Stream Temperature-Air Temperature Relationship

One line of evidence that groundwater contributions to the stream may be different in the spring months than in the fall months during storms is an examination of the relationship between stream temperature and air temperature on a seasonal scale. Figure 5-3 below presents this relationship for the study stream, highlighting the difference between data collected in the spring months (red points) and data collected in the fall months (blue points).

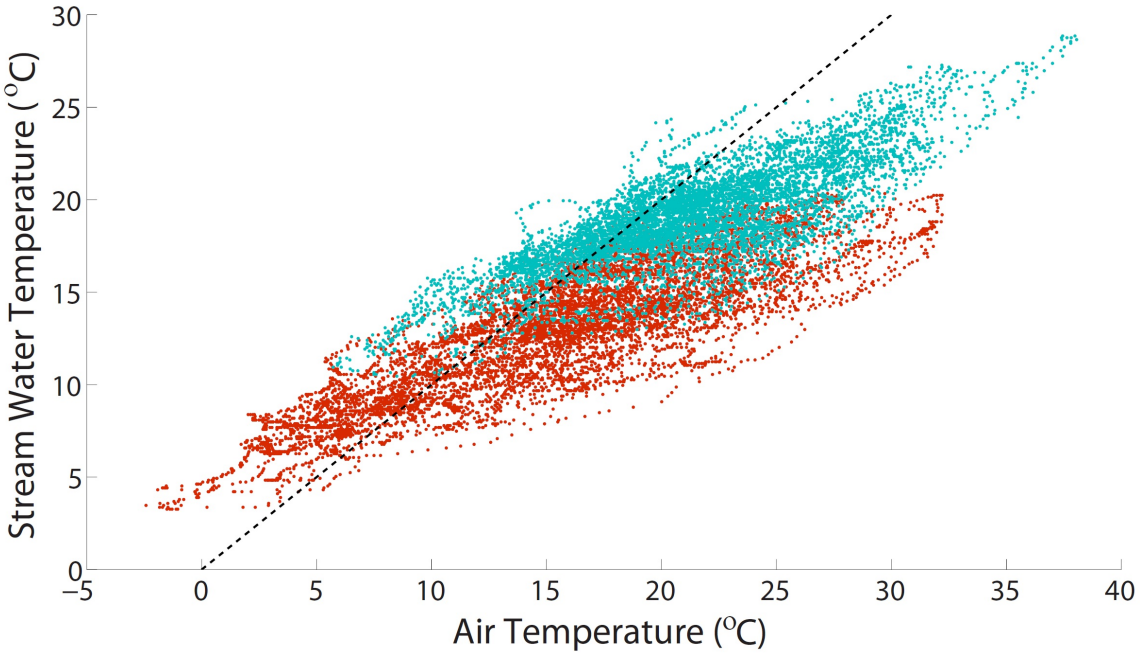

Figure **5-3**: Relationship between water temperature and air temperature both for spring data (April through June 2011, red points) and fall data (July through September, blue points). The dashed line is a 1:1 reference line.

The slopes and intercepts for the best fit lines through both the spring and fall data can provide insight into whether groundwater is a strong control on stream temperature in this system. Streams that are more controlled by climatic conditions have steeper slopes and lower intercepts (closer to the 1:1 line in Figure 5-3), while streams that depend more on groundwater input have lower slopes and larger intercepts (*O'Driscoll and DeWalle, 2006*). For comparison,

we superimpose the slope-intercept points for this study stream during spring and fall conditions on top of the slope-intercept relationships studied by O'Driscoll and DeWalle *(2006)* in the nearby Spring Creek watershed in Centre County, PA (Figure 5-4).

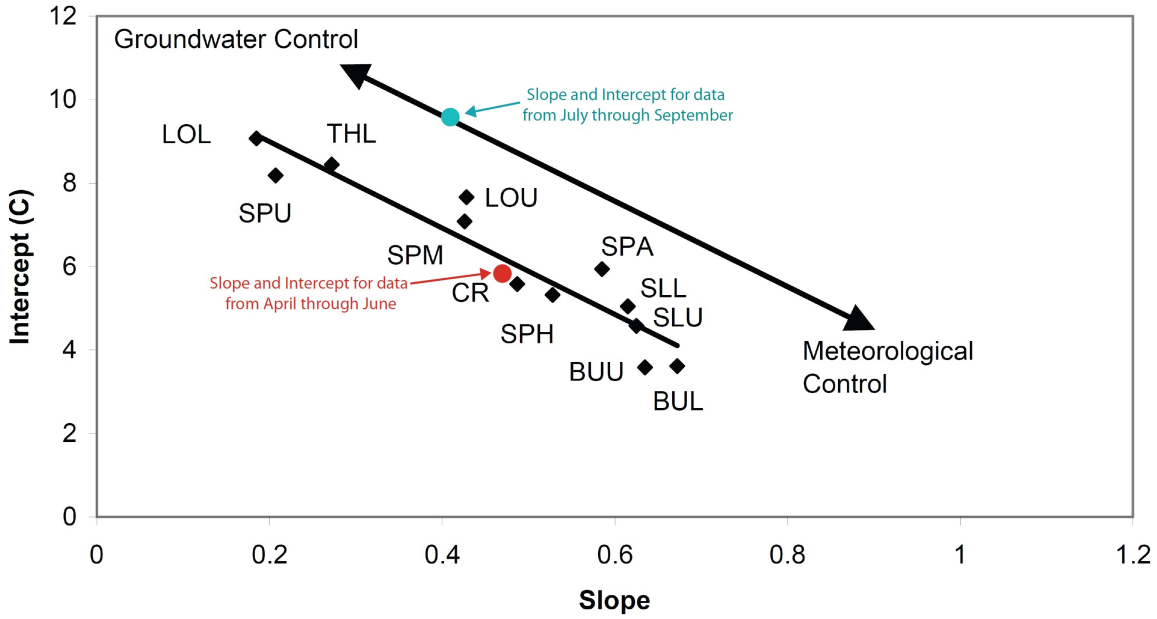

Figure **5-4**: Modified from O'Driscoll and DeWalle (*2006*), the study stream's slope-intercept data plotted on top of the relationships for 12 study locations within the Spring Creek basin in Centre County, PA.

The slope-intercept relationship for the spring data plots differently than the slope-intercept relationship for the fall data (Figure 5-4). The conceptual relationship (the black line with arrows pointing to groundwater control and meteorological control) shown in O'Driscoll and DeWalle (*2006*) would suggest that this stream is more impacted by groundwater contributions in the fall while its thermal regime is more controlled by meteorological conditions in the spring. This conclusion is somewhat muddled as both air temperature and water temperature tend to be higher in the fall months (July through September), which affects the slope and intercept of the best fit lines for the data.

Chapter 6

Conclusions

We have observed storms that cause rapid stream temperature increases of up to 3.8 °C in a rural headwater stream as well as trends over six months that suggest that storms may more often cause increases in stream temperature than previously thought in rural settings. These increases in stream temperature can occur at any time of day, but occurred with more likelihood during the spring months (April through June). The largest changes in stream temperature during storms (whether positive or negative) consistently occurred with storms that either produced large amounts of rain or were very intense (or both). These observations suggest that while the stream sometimes behaves as predicted by previous work (particularly in the fall months when large storms produce larger decreases in temperature), there are times where the current understanding does not fit this system. Instead, we have several lines of evidence that point to event flow in the stream being composed of "new" water (either from runoff or direct precipitation) rather than "older" groundwater being displaced into the stream as predicted.

It seems most likely that the primary physical mechanism for the stream's response to this storm event is overland flow. With the high precipitation intensity and low soil permeability, overland flow is likely to occur and relative to subsurface inflow, it occurs over a much shorter timescale (Dingman, 2008). This finding points to a need for more research on the thermal response to storms in other streams with similar low-permeability soils and poor connections to groundwater. Combined with warmer temperatures in a humid environment that produces

warmer precipitation, these “urban-like” stream temperature responses may occur more often than previously thought.

This study also has implications for techniques used to separate hydrographs in hillslope hydrology. Recent field studies use a wide variety of water quality parameters and flow measurements to separate contributions of runoff mechanisms to storm event flow in streams (Appendix I). However, temperature is little used as a separation basis even though heat has become a fairly common tracer in groundwater-surface water studies within the last decade. We have shown that temperature could also be used in end-member analyses to learn more about the sources of runoff to a stream. This study may open a door into considering temperature analyses as another line of evidence in hillslope hydrology. This is especially poignant as advances in technology have made it easy and inexpensive to take high resolution temperature data both in space and time.

If there were an opportunity to complete more fieldwork related to this project, flumes or weirs could be used to gather continuous flow measurements at two locations along the stream. The discharge record is critical for end-member analyses as well as for any future modeling work related to these observations. A continuous flow record collected at multiple locations would also allow for a mass balance analysis of the reach, which might help in determining the location and timing of input to the stream. If it were impossible to collect continuous discharge data, three to five stage loggers would be installed along the stream reach with multiple surveys at each logger’s cross-section. Stream temperature and electrical conductivity data would also be collected simultaneously at three more locations upstream (particularly in the headlands of the stream). Finally, collecting climatic data within the drainage area of the study site would reduce uncertainty in our analyses.

References

Agersborg, H. P. (1930), The influence of temperature on fish, *Ecol.*, 11, 136-144.

Alexander, R. B., E. W. Boyer, R. A. Smith, G. E. Schwarz, and R. B. Moore (2007), The role of headwater streams in downstream water quality*, J. Amer. Water Resour. Assoc.*, 43(1), 41-59,doi: 10.1111/j.1752-1688.2007.00005.x.

Arismendi, I., S. L. Johnson, J. B. Dunham, R. Haggerty, and D. Hockman-Wert (2012), The paradox of cooling streams in a warming world: Regional climate trends do not parallel variable local trends in stream temperature in the Pacific continental United States, *Geophys. Res. Lett.,* 39, L10401, doi:10.1029/2012GL051448.

Brown, L. E. and D. M. Hannah (2006), Alpine stream temperature response to storm events, *J. Hydrometeorol.*, 8, 952-967, doi: 10.1175/JHM597.1.

Chow, V. T., D. R. Maidment, and L. W. Mays (1988), *Applied Hydrology*. McGraw-Hill, New York.

Dicken, C. L., S. W. Nicholson, J. D. Horton, S. A. Kinney, G. Gunther, M. P. Foose, and J. A. L. Mueller (2008), Preliminary integrated geologic map databases for the United States: Delaware, Maryland, New York, Pennsylvania, and Virginia, *U.S. Geol. Surv. Open-File Report 2005-1325.*

Dingman, S. L. (2008), *Physical Hydrology*. Waveland Press, Long Grove, Illinois.

Doden, A. G. and D. P. Gold (2008), Bedrock geologic map of the McAlevys Fort quadrangle, Huntingdon, Centre, and Mifflin counties, Pennsylvania, *Penn. Geol. Surv., 4th Ser., Open File Report OFBM 08-02.0,* 22 pp.

Fulton, J. W., E. H. Koerkle, S. D. McAuley, S. A. Hoffman, and L. F. Zarr (2005), Hydrogeologic setting and conceptual hydrologic model of the Spring Creek Basin, Centre County, Pennsylvania, *U.S. Geol. Surv. Sci. Invest. Rep., 2005-5091,* 83 pp.

Hogg, I. D., D. D. Williams, J. M. Eadie, and S. A. Butt (1995), The consequences of global warming for stream invertebrates: A field simulation, *J. Therm. Biol.*, 20 (1/2), 199-206.

Homer, C. C., L. Y. Huang, B. Wylie, and M. Coan (2004), Development of a 2001 National Landcover Database for the United States, *Photogramm. Eng. Remote Sens.,* 70 (7), 829-840.

Jin, L., R. Ravella, B. Ketchum, P. R. Bierman, P. Heaney, T. White, and S. L. Brantley (2010), Mineral weathering and elemental transport during hillslope evolution at the Susquehanna/Shale Hills Critical Zone Observatory, *Geochim. Cosmochim. Acta*., 74(13), 3669-3691, doi: 10.1016/j.gca.2010.03.036.

Jones, M. P. and W. F. Hunt (2009), Bioretention impact on runoff temperature in trout sensitive waters, *J. Environ. Eng.*, 135(8), 577-585,doi: 10.1061/(ASCE)EE.1943-7870.0000022.

Jones, M. P. and W. F. Hunt (2010), Effect of storm-water wetlands and wet ponds on runoff temperature in trout sensitive waters, *J. Irrig. Drain. Eng.*, 136(9), 656-661, doi: 10.1061/_ASCE_IR.1943-4774.0000227.

Kaushal, S.S., G.E. Likens, N.A. Jaworski, M.L. Pace, A.M. Sides, D. Seekell, K.T. Belt, D. Secor, and R. L. Wingate (2010). Rising stream and river temperatures in the United States. *Frontiers in Ecol. and the Envir.*, 8(9), 461-466.

Kim, K. S. and S. C. Chapra (1997), Temperature model for highly transient shallow streams, *J. Hydraul. Eng.*, 123(1), 30-40, doi: 10.1061/(ASCE)0733-9429(1997)123:1(30).

Kirkby, M. (1988), Hillslope runoff processes and models, *J. Hydrol.,* 100 (1-3), 315-339.

Linsley, R. K. and M. A. Kohler (1951), Predicting the runoff from storm rainfall, *U.S. Weather Bureaur Research Paper 34*, 13 pp.

Logue, J., P. Tiku, and A. R. Cossins (1995), Heat injury and resistance adaption in fish, *J. Therm. Biol.*, 20 (1/2), 191-197.

Lowe, W. H. and G. E. Likens (2005), Moving headwater streams to the head of the class, *BioSci.*, 55(3), 196-197, doi: 10.1641/0006-3568(2005)055[0196:MHSTTH]2.0.CO;2.

Mays, L. W. (2005), *Water Resources Engineering*. Wiley, John & Sons, Inc., Hoboken, New Jersey.

Natarajan, P. and A. P. Davis (2010), Thermal reduction by an underground storm-water detention system, *J. Envir. Eng.*, 136 (5), 520- 526, doi: 10.1061/_ASCE_EE.1943-7870.0000172.

Nelson, K. C. and M. A. Palmer (2007), Stream temperature surges under urbanization and climate change: data, models, and responses, *J. American Water Resources Association,* 43(2), 440-452, doi: 10.1111/j.1752-1688.2007.00034.x.

O'Driscoll, M. A. and D. R. DeWalle (2006), Stream-air temperature relations to classify stream-groundwater interactions in a karst setting, central Pennsylvania, USA, *J. Hydrol.,* 329(1-2), 140-153, doi: 10.1016/j.jhydrol.2006.02.010.

Pennsylvania State Climatologist (2012), Interactive Data Archive: University Park, Pa., Pennsylvania State University College of Earth & Mineral Sciences, accessed June 19, 2012, at *http://climate.met.psu.edu/www_prod/data/state/regional.php*.

Reese, S. O. and D. W. Risser (2010), Summary of groundwater-recharge estimates for Pennsylvania, *Penn. Geol. Surv., 4th Ser., Water Resour. Rep. 70,* 18 pp.

Shanley, J. B. and N. E. Peters (1988), Preliminary observations of streamflow generation during storms in a forested piedmont watershed using temperature as a tracer, *J. Contam. Hydro*., 3, 349-365.

Slingerland, R. L. and L. R. Kump (2011), *Mathematical Modeling of Earth's Dynamic Systems*. Princeton University Press, Princeton, New Jersey.

Smith, K. and M. E. Lavis (1975), Environmental influences on the temperature of a small upland stream, *Oikos: J. Ecol*., 26(2), 228-236.

Stuckey, M. H. and S. A. Hoffman (2010), Pennsylvania Stream Stats – A web-based application for obtaining water-resource-related information, *U.S. Geol. Surv. Fact Sheet 2010-3086,* 2 pp. Application available online at http://streamstats.usgs.gov/pennsylvania.html /.

Stull, R. (2011), Wet-bulb temperature from relative humidity and air temperature, *J. App. Met.Clim.*, doi: 10.1175/JAMC-D-11-0143.1.

U.S. Natural Resources Conservation Service (2012), Web Soil Survey, *Soil Survey Staff of the Department of Agriculture*. Available online at http://websoilsurvey.nrcs.usda.gov/.

U.S. Soil Conservation Service (1972), Hydrology, Section 4, *SCS National Engineering Handbook.* Available from U.S. Government Printing Office, Washington, DC.

U.S. Soil Conservation Service (1986), Urban Hydrology for Small Watersheds, *Tech. Release No. 55*. Available from U.S. Government Printing Office, Washington, DC.

Woodruff, J. F. and J. D. Hewlett (1970), Predicting and mapping the average hydrologic response for the eastern United States. *Water Resources Research,* 35: 2469-2485.

Appendix A

Mean Monthly Air Temperature and Precipitation Data

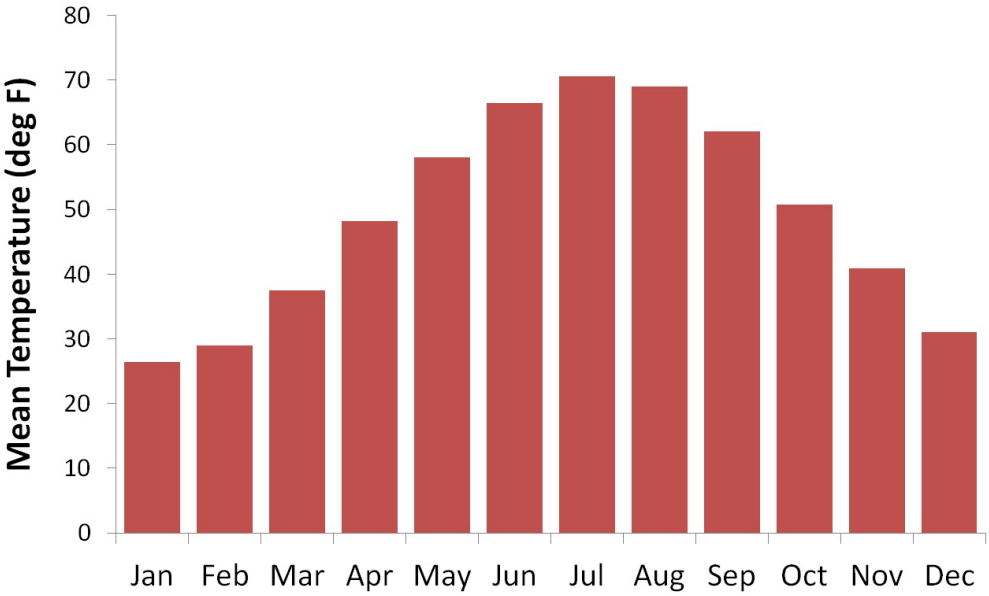

Figure **A-1**: Average monthly air temperature for surrounding region (data collected from 1899 to 2012 in region 8) (Pennsylvania State Climatologist, 2012)

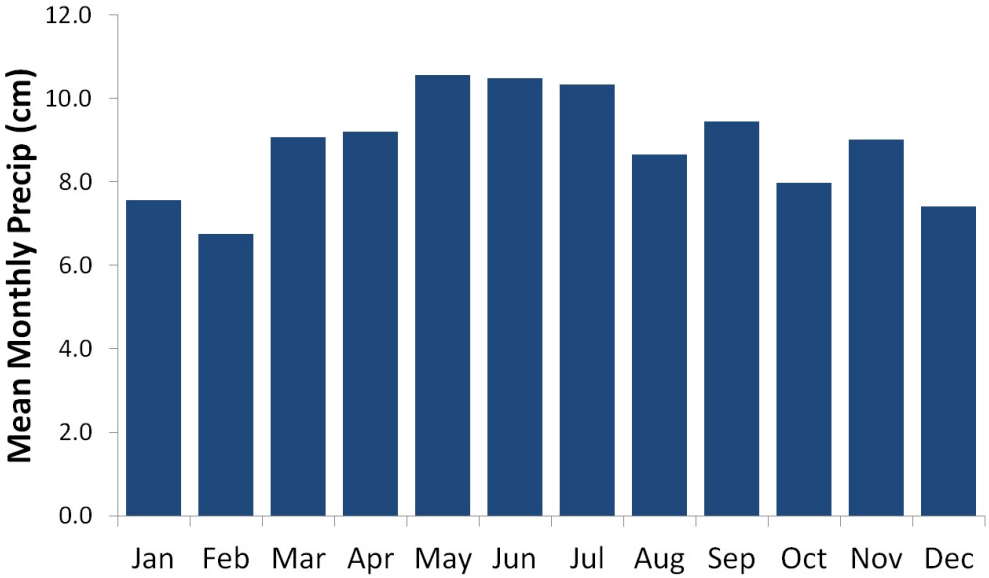

Figure **A-2**: Average monthly precipitation for surrounding region (data collected from 1989 to 2012 in region 8) (Pennsylvania State Climatologist, 2012)

Appendix B

Empirical Estimation of Wet Bulb Temperature

Inverse relationship from *Stull, 2011* to calculate wet bulb temperature as a function of air temperature and relative humidity:

$$Tw = Tair \cdot \text{atan}[0.151977 \cdot (RH\% + 8.313659)1/2] + \text{atan}(Tair + RH\%) - \text{atan}(RH\% - 1.676331) + 0.00391838 \cdot (RH\%)3/2 \cdot \text{atan}(0.023101 \cdot RH\%) - 4.686035 \quad \text{Eqn. B-1}$$

where *Tw* is the wet bulb temperature, *Tair* is the air temperature, and *RH%* is the percent relative humidity.

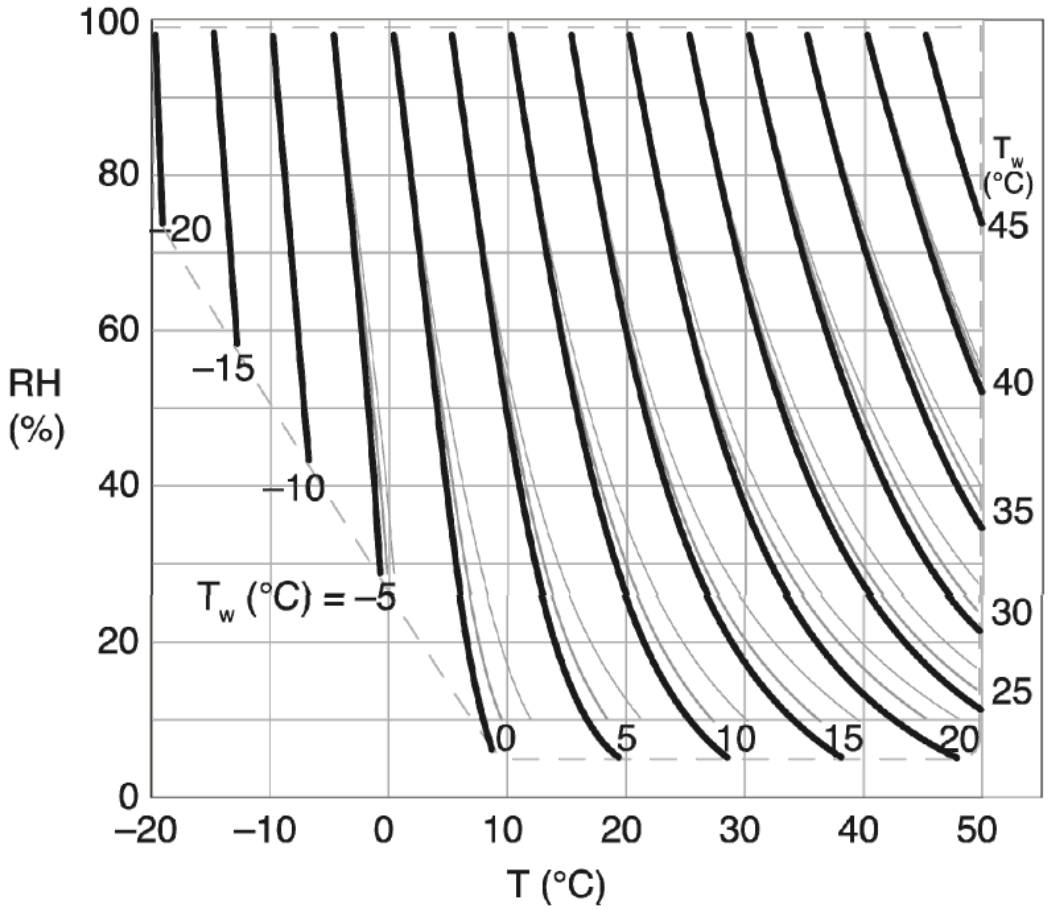

Figure **B-1** – From *Stull 2011*, Isopleths of wet-bulb temperature *Tw* (thick black curves) vs. relative humidity (*RH%*) and air temperature *T*, found with the empirical relationship.

The valid range is enclosed by a dotted line, and the valid pressure is 101.325 kPa. The grey curves associated with each *Tw* are for *P* = 80 kPa (thinner line) and *P* = 60 kPa (thinnest line). These grey curves (not found from eq. 1) are useful for estimating the error if eq. (1) is applied to pressures not equal to *P* = 101.325 kPa.

Appendix C

Estimates of Discharge from a Stream Stage Record

At this field site we were unable to continuously record discharge for several reasons. First, the managers of the land strongly preferred that there be no permanent construction on the stream, primarily because this field site is a part of the lakebed of a drained reservoir that may be filled within the year. This made it impossible to install any flume or weir type device to measure discharge continuously.

We also were unable to accurately measure discharge with a flowmeter or acoustic doppler velocimeter (ADV) across a wide spectrum of discharges. At low flows, the stream is too narrow and too shallow for accurate flowmeter or ADV measurements. During large storms, the stream is highly dynamic making it difficult to capture estimates of these higher magnitude flows. If we had been able to make frequent measurements, we would have correlated our manual flow estimates with the continuous stage record to establish a stage-discharge rating curve.

Without this stage-discharge rating curve, we were forced to estimate the discharge using Manning's equation and other estimated stream parameters. From survey data, we estimated that the bed slope of the stream reach was 0.009. We were also forced to estimate the Manning's *n* for the reach. As mentioned, this stream is highly dynamic. During low flows, vegetation grows in the channel bed greatly increasing the roughness coefficient. During higher flows the roughness coefficient is reduced. During floods that force the stream to flow out of its banks, the roughness coefficient is once again increased. While it's impossible to accurately estimate this coefficient, we chose coefficient values that enabled our estimated flow record to best fit the 12 manual discharge observations that we did collect. During times of high flow (spring months), we used a Manning's *n* of 0.05, which is the recommended roughness coefficient for natural minor streams (top width at flood stage is less than 100 feet) (*Mays, 2005*). During times of lower flow (summer months), we used a Manning's *n* of 0.10 which is recommended for very weedy reaches of natural minor streams (*Mays, 2005)*. For times of out-of-bank flooding, we used a Manning's coefficient that ranged between 0.10 and 0.30, which is within the range recommended for overland flow through grasses (*Mays, 2005*).

Over the course of our fieldwork, we surveyed the field site three times. Each time we always took a careful survey of the stream cross-section where our stage logger collected data. Using these data, we plotted the cross-sectional profile of the stream at the point where stage

data is collected. We then used the location of the logger and the water depth observed to determine what cross-sectional area of the channel would be filled with water at each moment in time. Using Matlab we were able to determine the area, wetted perimeter, and hydraulic radius from the survey and stage data through time. With these calculations we were able to estimate a continuous discharge record using Manning's Equation as shown below

$$Q = A \cdot n^{-1} \cdot R_h^{2/3} \cdot S_o^{1/2} \qquad \text{Eqn. C-1}$$

where Q is discharge, A is the cross-sectional area of the channel, n is the Manning's roughness coefficient for the stream channel, R_h is the hydraulic radius of the channel, and S_o is the channel bottom slope (∂z/∂x).

See Figure 2-3 for the best estimation of the continuous flow record as calculated using equation C-1. Estimates of flow range between 0.007 cms in mid-June to 1.29 cms during a large storm at the end of April. Without any significant rain (more than 1 mm), between June 24th and July 25th, baseflow recession occurred where estimated discharge steadily dropped from 0.086 cms to 0.007 cms over the 4 weeks. During this time period, a daily cycle becomes apparent in the scalloped oscillations seen in Figure 2-3. This daily cycle had an average amplitude of 0.002 cms.

Unfortunately, our estimates of flow during peak storm discharges are the most uncertain estimates. Without manual measurements or accurate estimates of the Manning's roughness coefficient, these estimates are difficult to trust conclusively. This is especially difficult as these storm discharges are key to our better understanding the stream temperature responses we observe to storm events.

Appendix D

Kinematic Wave Routing of Storm Flow

Introduction

The objective of this study was to create a flow routing module to predict discharge (Q) through time and space along a headwater stream during large storms. To solve for discharge along this stream reach, we use St. Venant's Equation, coupled with conservation of mass, to numerically solve for the temporal and spatial evolution of the system. This mathematical model was derived using the steps outlined in Table 1.1 of *Slingerland and Kump, 2011*.

Physical Picture

We consider a small headwater stream in central Pennsylvania. This stream is an unnamed tributary to Shaver's Creek in Huntingdon County, PA. The watershed is approximately 1.5 km^2 and is 92% forested. The stream has an average bed slope of 0.009 and an average stream width of 1 meter. We aim to model discharge over a 200 meter reach of the stream. For modeling purposes, we approximate the stream channel as rectangular. Figure D-1 below shows the physical picture of the rectangular stream channel including discharge (Q), lateral inflow (q), stream width (W), stream stage (h), and bed slope angle (α).

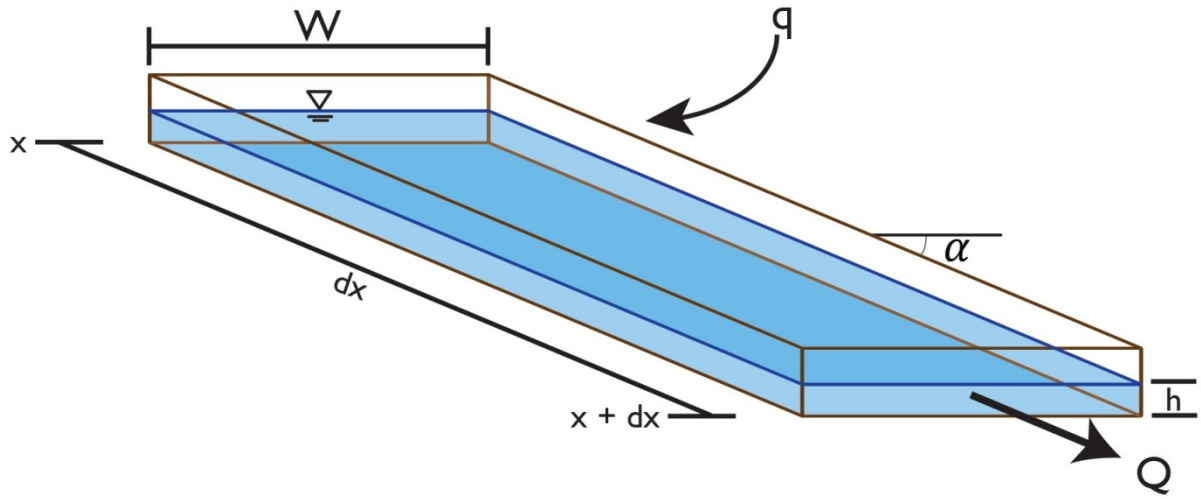

Figure **D-1**: Schematic of the physical system showing the approximate shape of the river channel, the still water depth (h), and the free surface elevation (Z).

Variables

- Q is the instantaneous discharge and is $f(x,t)$ [$m^3 s^{-1}$]
- h is the cross-sectional average water height and is $f(x,t)$ [m]
- A is the cross sectional area of the channel and is $f(x,t)$ [m^2]
- U is the water velocity and is $f(x,t)$ [$m\ s^{-1}$]

- W is the channel width [m]
- n is the Manning's roughness coefficient for the stream channel
- α is the stream channel bed slope angle
- S_o is the channel bottom slope (∂z/∂x)
- S_f is the friction slope and is derived from Manning's equation
- P_{wetted} is the wetted perimeter of the channel [m]
- R_H is the hydraulic radius of the channel equal to A/P_{wetted} [m]
- x is the axis of the channel [m]
- t is time [sec]

Physical Laws

With two unknowns (discharge and area) in time and space, two laws are applied to this problem: (1) conservation of mass and (2) St. Venant's Equation for 1D, vertically integrated, unsteady, non-uniform flow in a variable cross-section. Manning's Equation will also be used to describe the friction force. *Note: Velocity (V) and water surface elevation (h) are also dependent variables, but are related to the discharge and area and can be solved by the following equations: Q = VA and A = hW*.

Restrictive Assumptions

(1) Flow is one-dimensional and depth and velocity vary only in the longitudinal direction of the channel, therefore the system can be represented as 1D in the x-direction
(2) This problem is unsteady in time and non-uniform in the x-direction
(3) Longitudinal axis of the channel is approximately straight and channel can be approximated as rectangular
(4) Hydrostatic pressure prevails and vertical accelerations can be neglected (flow varies gradually along the channel)
(5) Processes like scour and deposition can be neglected (the bottom slope of the channel is small and the channel bed is fixed)
(6) Internal particle friction, friction due to wind shear, and energy loss through eddy motion can be ignored
(7) There are no sources or sinks of water (no lateral inflows)
(8) The channel is narrow enough such that Coriolis accelerations may be ignored
(9) Manning's equation can be used to describe resistance effects (use resistance coefficients from steady uniform turbulent flow)
(10) The fluid is incompressible and of constant density, ρ
(11) Channel wetted perimeter can be approximated as being constant at 1.5 meters
(12) Channel bed slope can be approximated as being constant at 0.009
(13) The Manning's n can be approximated as being constant at 0.101

Mass and Momentum Balances

The mass balance for the flow of water through the channel is:

$$\text{TROCM} = \text{MRI} - \text{MRO} \pm \Sigma \text{ Sources/Sinks} \qquad \text{Eqn. D-1}$$

In other words, the time rate of change in mass is equal to the mass rate in minus the mass rate out plus sources minus sinks. When including lateral inflow as a source of mass, this equation in symbols can be written as:

$$\frac{\partial}{\partial t}\rho A dx = Q\rho - \left[Q\rho + \frac{\partial}{\partial x}Q\rho dx\right] + \rho q_L dx \qquad \text{Eqn. D-2}$$

Starting with the simplest case, we assume there is no lateral inflow and this equation reduces to the following:

$$\frac{\partial A}{\partial t} + \frac{\partial Q}{\partial x} = 0 \qquad \text{Eqn. D-3}$$

When like units are canceled out, the equation simplifies to a dimensionally homogeneous expression where every term has units of *m^2 per second*. Moving on to conservation of momentum, the St. Venant's equation for1D, unsteady, vertically integrated, non-uniform flow through the channel is:

$$\text{TROCMom} = \text{MomRI} - \text{MomRO} \pm \Sigma \text{ Sources/Sinks} \qquad \text{Eqn. D-4}$$

In other words, the time rate of change in momentum is equal to the momentum rate in minus the momentum rate out plus sources minus sinks. In symbols, this equation is:

$$\frac{\partial}{\partial t}\rho A dx V = Q\rho V - \left[Q\rho V + \frac{\partial}{\partial x}Q\rho dx V\right] + \Sigma F_x \qquad \text{Eqn. D-5}$$

If we quickly check units on this equation, we see that every term has consistent units of kg m s^{-2} or Newtons. Canceling like terms and dividing through by (ρdx) in each term, we are left with:

$$\frac{\partial AV}{\partial t} + \frac{\partial QV}{\partial x} = \frac{\Sigma F_x}{\rho dx} \qquad \text{Eqn. D-6}$$

We need to define the sum of forces on the right-hand side of the equation. The sum of forces could include gravity along the channel, energy loss through eddy motion, wind shear along the water surface, pressure, and friction created by shear stress along the bottom and sides of the channel. As shown below (and mentioned in the assumptions), we will only consider friction, gravity, and pressure.

$$\Sigma F_x = F_{gravity_x} + F_{pressure_x} + F_{friction_x} \qquad \text{Eqn. D-7}$$

We can define the gravity force along the channel to be:

$$F_{gravity} = \rho \cdot g \cdot A \cdot \sin\alpha \cdot dx = \rho \cdot g \cdot A \cdot S_o \cdot dx \quad \textit{where} \quad S_o = -\frac{\partial z}{\partial x} \qquad \text{Eqn. D-8}$$

S_o is the channel bottom slope (change in elevation divided by the change in distance along the x-axis). Next, we can define the net hydrostatic pressure force as a balance of pressure force out subtracted from the pressure force in:

$$F_{pressure_x} = \overline{P}_x A - \left[\overline{P}_x A + \frac{\partial}{\partial x}\overline{P}_x A dx\right] = -\frac{\partial}{\partial x}\overline{P}_x A dx \quad \textit{where} \quad \overline{P}_x = \frac{1}{2}\rho g h \qquad \text{Eqn. D-9}$$

Finally, we can define the friction drag force as:

$$\mathrm{F_{friction_x}} = -\tau_{o_x} \cdot \ell \cdot \mathrm{dx} = -\rho \cdot \mathrm{g} \cdot \mathrm{A} \cdot \mathrm{S_f} \cdot \mathrm{dx} \qquad \text{Eqn. D-10}$$

S_f is the friction slope and will be derived from Manning's equation. Therefore the sum of forces is equal to:

$$\Sigma \mathrm{F_x} = -\rho \mathrm{gA} \frac{\partial \mathrm{z}}{\partial \mathrm{x}} \mathrm{dx} - \rho \mathrm{gA} \frac{\partial h}{\partial x} dx - \rho \mathrm{gAS_f dx} \qquad \text{Eqn. D-11}$$

When this sum of forces is plugged into the momentum equation above, the 1D St. Venant Equation becomes:

$$\frac{\partial \mathrm{Q}}{\partial \mathrm{t}} + \frac{\partial \mathrm{QV}}{\partial \mathrm{x}} + \mathrm{gA}\left(\frac{\partial h}{\partial x} + \frac{\partial \mathrm{z}}{\partial \mathrm{x}} + \mathrm{S_f}\right) = 0 \qquad \text{Eqn. D-12}$$

The units of this equation are homogeneous and are in $m^3 s^{-2}$. From left to right, the terms of the equation include local acceleration, advective acceleration, pressure force, gravity force, and the friction force terms. This equation can be simplified into a few different forms depending on how many terms of the equation are included. The dynamic wave includes all of the terms shown above. The diffusion wave neglects both acceleration terms. The kinematic wave neglects all of the terms but the gravitational and friction force terms.

Though this may seem too simple, the kinematic wave does a good job of flow routing when the system does not include tides, tributary inflows, or reservoir operations (*Chow et al., 1988*). It is also recommended that the bed slope of the channel be greater than 0.001. The kinematic wave assumes that the friction force (S_f) is balanced by the gravitational force (S_o). Because $S_o = S_f$, we can substitute the bed slope into Manning's equation as shown below:

$$Q = \left(\frac{S_o^{1/2}}{nP^{2/3}}\right) A^{5/3} \qquad \text{Eqn. D-13}$$

Solving for the area, *A*, we get that :

$$A = \alpha = \left[\frac{nP^{2/3}}{\sqrt{S_o}}\right]^{0.6} \quad \text{and} \quad \beta = 0.6 \qquad \text{Eqn. D-14}$$

The continuity equation shown in equation D-3 has two dependent variables (discharge and area). Using α and β, the area can be eliminated from the continuity equation by differentiating Manning's equation:

$$\frac{\partial A}{\partial t} = \alpha\beta Q^{\beta-1} \frac{\partial Q}{\partial t} \qquad \text{Eqn. D-15}$$

Substituting this equation into the continuity equation, we get the kinematic wave equation:

$$\frac{\partial Q}{\partial x} + \alpha\beta Q^{\beta-1} \frac{\partial Q}{\partial t} = 0 \qquad \text{Eqn. D-16}$$

Interval of Interest

Temporally we consider this problem from 0 < t < 43,200 seconds (12 hours), where t_o is May 23rd, 2011 at 14:00 and t_{final} is May 24th, 2011 at 02:00. Spatially we consider this problem from 0 < x < 200 m as this is the approximate length from the stream data logger (boundary

condition) to the study site. Temporal and spatial steps were set in such a way as to ensure stability of the explicit scheme: *Δt = 10 second* and *Δx = 25 meters.*

Initial Conditions

Since the time derivative is first-order, we only need one initial condition. The initial condition for this problem would be $Q(x,0) = 0.05\ m^3\ s^{-1}$. This number comes from data collected at the field site during the time period of interest.

Boundary Conditions

Since the spatial derivative is first-order, we only need one boundary condition. The initial condition for this problem would be $Q(0,t) = Q_{data}$. This condition will be satisfied by feeding the model discharge data estimated from a stage logger located in the study reach. For more detail on the estimation of discharge from stage, see Appendix C.

Numerical Scheme

We use a linear explicit scheme with the stencil shown below in Figure D-2 (*Chow et al., 1988*) to solve the kinematic wave equation shown in Equation 15. Both the spatial and temporal derivatives of discharge are found using the backward-difference. The value of Q in the term $\alpha\beta Q^{\beta-1}$ is approximated as an average of Q^{j+1} and Q_{i+1} (Figure D-2). This keeps the equation linear.

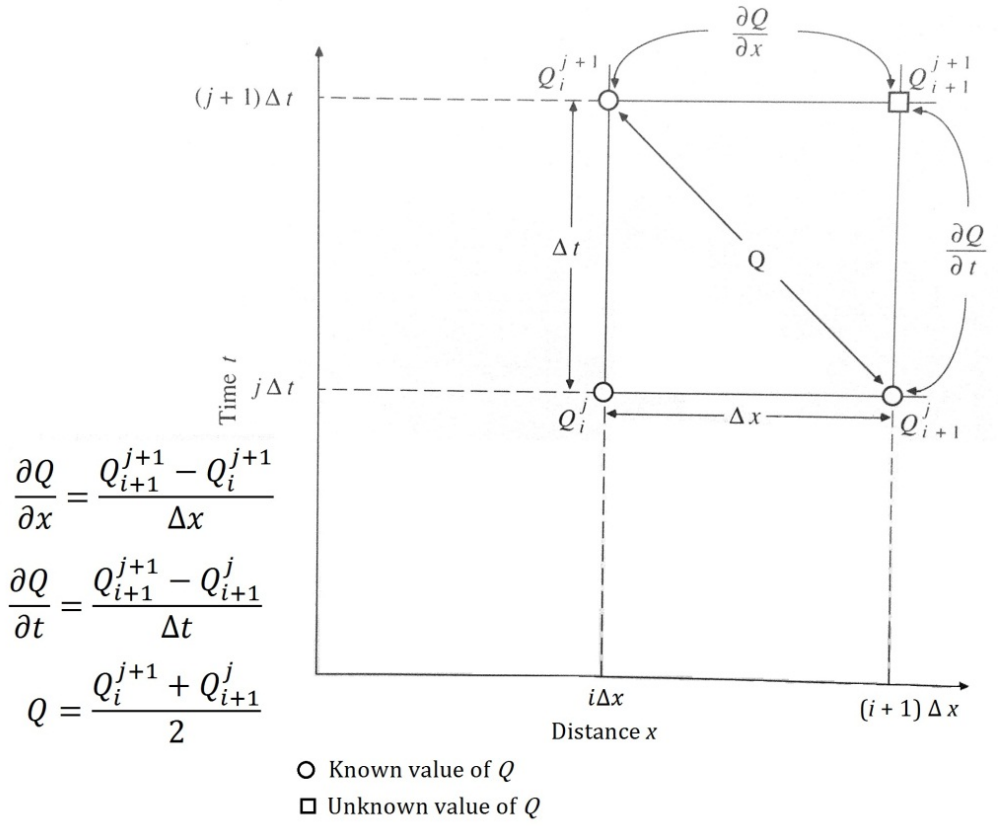

$$\frac{\partial Q}{\partial x} = \frac{Q_{i+1}^{j+1} - Q_i^{j+1}}{\Delta x}$$

$$\frac{\partial Q}{\partial t} = \frac{Q_{i+1}^{j+1} - Q_{i+1}^{j}}{\Delta t}$$

$$Q = \frac{Q_i^{j+1} + Q_{i+1}^{j}}{2}$$

Figure **D-2**: Finite difference stencil for the linear explicit kinematic wave equation (adapted from *Chow et al., 1988*)

Substitute the finite difference terms into the kinematic wave equation, we are left with:

$$\frac{Q_{j+1}^{i+1}-Q_j^{i+1}}{\Delta x}+\alpha\beta\left(\frac{Q_{j+1}^{i}+Q_j^{i+1}}{2}\right)^{\beta-1}\left(\frac{Q_{j+1}^{i+1}-Q_{j+1}^{i}}{\Delta x}\right)=0 \qquad \text{Eqn. D-17}$$

Of note, I switched *i* and *j* to be opposite of what is shown in Figure D-2 so that *i* is associated with time and *j* is associated with distance. When solving for $Q^{i+1}{}_{j+1}$, the equation resolves to:

$$Q_{j+1}^{i+1}=\frac{\left[\frac{\Delta t}{\Delta x}Q_j^{i+1}+\alpha\beta Q_{j+1}^{i}\left(\frac{Q_{j+1}^{i}+Q_j^{i+1}}{2}\right)^{\beta-1}\right]}{\left[\frac{\Delta t}{\Delta x}+\alpha\beta\left(\frac{Q_{j+1}^{i}+Q_j^{i+1}}{2}\right)^{\beta-1}\right]} \qquad \text{Eqn. D-18}$$

The Courant-Fredericks-Levy stability criteria shown below is a requirement for the stability of this scheme:

$$\left|\frac{\Delta t\sqrt{gh_{max}}}{\Delta x}\right|\leq 1 \qquad \text{Eqn. D-19}$$

The maximum stage (h_{max}) during the storm was 0.625 meters and *g* is the acceleration due to gravity and is equal to 9.8 m^2/s. With a Δt = 10 second and Δx = 25 meters, the Courant-Fredericks-Levy criteria is met since the CFL value for this model is 0.9899.

Results

With the given scheme and parameters above, the model produced the following results. Figure D-3 below shows the calculated hydrographs at 50 meters, 100 meters, 150 meters, and 200 meters downstream of the boundary condition hydrograph through time.

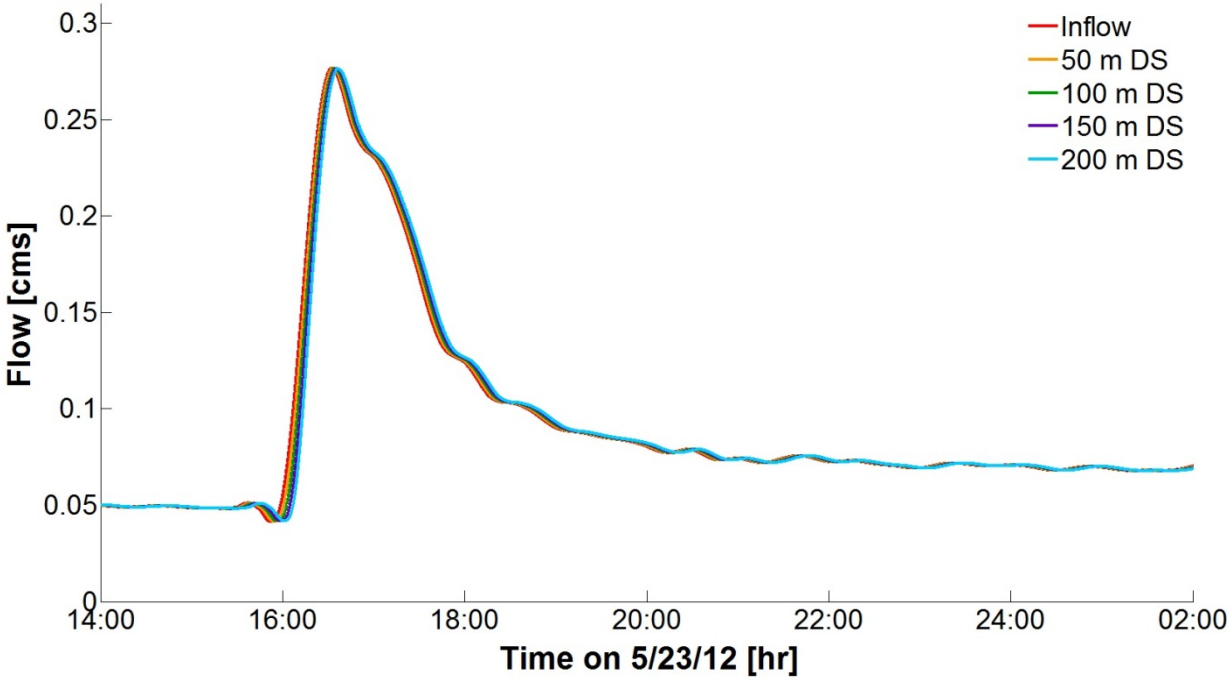

Figure **D-3**: Model output showing discharge through time for five locations (as well as at the boundary).

Though it appears there isn't much change in the flood wave's position in Figure D-3, the peak discharge at 200 meters downstream of the boundary condition occurs 4.3 minutes after the peak discharge at the boundary condition. 1000 meters downstream from the boundary condition, the peak discharge arrives 21.5 minutes after the peak discharge at the boundary condition. This short travel time is consistent with the range of observations we've made with conservative salt slug tests.

The mean velocity of the kinematic wave in this system is 2.79 kilometers per hour or 0.775 meters per second. Over 200 meters, the peak flow attenuates by 0.000033 cms or 0.01%. Over 1000 meters, the peak flow attenuates by 0.0005 cms or 0.18%. This is such a small attenuation that we can make the reasonable assumption for the heat transport module that there is no dispersion of the flood wave through space or time in the reach.

Appendix E

Summary Data for All Storms Observed

Table **E-1**: Summary data for all observed storms including storm date, total precipitation, storm duration, mean storm intensity, and observed stream temperature change.

Storm Date	Total Precip (mm)	Storm Duration (hr)	Mean Intensity (mm/hr)	Temp Change (°C)
04/03/11	1.9	1.17	1.63	-0.50
04/04/11	11.2	2.83	3.95	-0.69
04/05/11	8.8	6.67	1.32	-1.01
04/08/11	25.9	13.33	1.94	-0.51
04/11/11	4.3	0.67	6.45	0.10
04/12/11	5.2	3.17	1.64	-0.49
04/12/11	2.3	2.67	0.86	-0.40
04/12/11	1.1	1.17	0.94	-0.20
04/13/11	11.4	6.83	1.67	-0.10
04/16/11	22.8	12.67	1.80	0.10
04/19/11	3.6	1.83	1.96	0.50
04/19/11	1.5	0.83	1.80	0.00
04/19/11	6.1	2.00	3.05	-0.10
04/22/11	3.1	3.50	0.89	-0.20
04/22/11	2.4	4.33	0.55	-0.20
04/23/11	4.3	1.83	2.35	-0.10
04/25/11	1.6	0.50	3.20	-0.19
04/26/11	11.4	0.83	13.68	-1.05
04/26/11	7.3	1.50	4.87	-0.57
04/28/11	35.8	3.67	9.76	3.45
05/01/11	3.6	3.67	0.98	0.20
05/03/11	22.5	1.33	16.87	1.24
05/03/11	3	1.17	2.57	-1.63
05/04/11	4.5	3.67	1.23	-0.49
05/14/11	1.1	0.50	2.20	-0.10
05/15/11	1.1	1.50	0.73	0.00
05/15/11	6.4	4.33	1.48	0.00
05/15/11	2.6	2.50	1.04	0.39
05/15/11	4.6	1.33	3.45	0.10
05/15/11	2.4	1.50	1.60	-0.48
05/17/11	1.2	0.33	3.60	0.00
05/17/11	1.6	0.67	2.40	0.00

Storm Date	Total Precip (mm)	Storm Duration (hr)	Mean Intensity (mm/hr)	Temp Change (°C)
05/17/11	3.8	3.17	1.20	0.58
05/17/11	1.1	1.00	1.10	0.19
05/17/11	2.7	1.83	1.47	0.00
05/18/11	16.4	6.17	2.66	-0.19
05/18/11	7.2	1.67	4.32	0.39
05/19/11	1.3	0.33	3.90	-0.10
05/20/11	4.5	4.17	1.08	0.58
05/20/11	1.2	0.33	3.60	-0.10
05/20/11	5.5	0.50	11.00	-0.10
05/23/11	2.1	1.33	1.57	0.00
05/23/11	29.9	0.83	35.88	3.82
05/26/11	2.2	0.17	13.20	0.00
05/26/11	10.1	1.83	5.51	0.38
05/27/11	5.7	1.83	3.11	0.57
05/27/11	18.4	4.67	3.94	0.86
05/28/11	1.2	0.67	1.80	-0.19
06/04/11	4.7	1.50	3.13	0.00
06/10/11	8.3	1.00	8.30	-1.14
06/10/11	17.1	2.33	7.33	-0.10
06/11/11	5.8	0.83	6.96	-0.38
06/16/11	5	1.83	2.73	0.10
06/16/11	7	0.50	14.00	0.29
06/20/11	15.2	1.67	9.12	-0.09
06/24/11	2.7	0.83	3.24	-0.48
07/25/11	9.4	2.00	4.70	0.00
07/25/11	10.9	0.67	16.35	-1.83
07/28/11	20.3	2.67	7.61	-0.76
07/28/11	1.6	1.00	1.60	0.00
08/03/11	3.9	2.17	1.80	-0.19
08/03/11	2.6	1.83	1.42	-0.57
08/06/11	2.7	0.33	8.10	0.00
08/06/11	6.3	0.83	7.56	0.00
08/06/11	5.2	2.33	2.23	-0.29
08/06/11	9.2	1.33	6.90	-0.10
08/07/11	3.6	0.33	10.80	0.38
08/09/11	3.5	1.83	1.91	0.00
08/09/11	1.9	0.67	2.85	0.19
08/13/11	1.9	0.67	2.85	0.10
08/14/11	4.4	2.17	2.03	0.29

Storm Date	Total Precip (mm)	Storm Duration (hr)	Mean Intensity (mm/hr)	Temp Change (°C)
08/14/11	11	0.83	13.20	-0.86
08/15/11	2.7	0.67	4.05	-0.76
08/19/11	5.2	1.33	3.90	0.29
08/25/11	5.3	3.33	1.59	0.76
08/27/11	2.1	0.33	6.30	-1.05
08/27/11	23.8	10.83	2.20	-1.14
09/01/11	2.1	1.00	2.10	0.10
09/04/11	3.7	1.00	3.70	-0.09
09/05/11	106.9	42.50	2.52	-3.33
09/07/11	2.1	2.00	1.05	0.00
09/08/11	6.6	1.33	4.95	0.09
09/08/11	3.2	0.67	4.80	-0.29
09/11/11	2.4	0.50	4.80	-0.38
09/14/11	5.6	0.67	8.40	-0.29
09/15/11	2.2	1.67	1.32	-0.57
09/15/11	4.6	3.17	1.45	-0.57

Appendix F

Runoff Mechanisms and Their Favorable Environmental Conditions

Table **F-1**: Environmental factors favoring hillslope event-response mechanisms where K_h* is saturated hydraulic conductivity (Source: Dingman, 2008).

Mechanism	Soils/Geology	Water Table	Topography	Vegetation	Water-Input Rate[a]
Hortonian overland flow	Low surface K_h^*	Deep	Steep slopes	Absent to sparse	High
Saturation overland flow	Slopes: High surface K_h^*, decreasing gradually or abruptly at shallow depth; Conditions of Figure 9-22. Valley bottoms: Low to high K_h^*	Near surface	Concave, convergent slopes; Wide valleys	Absent to abundant	Low to high
Ground-water mounding	Slopes: Deep soils with high surface K_h^*. Valley bottoms: High K_h^*. Silty soils enhance flow from pressurized capillary fringe	Slopes: Deep; Valley bottoms: Near surface	Concave slopes, wide valleys	Absent to abundant	Low to moderate
Perched ground water (sloping slab)	Slopes: High surface K_h^*, decreasing gradually or abruptly at shallow depth; Macropores present	Absent to present in high-K_h^* layer	Steep slopes; straight to convex	Absent to abundant	Low to moderate

[a]Relative to K_h^*.

Appendix G

Estimated Velocity for Overland Flow

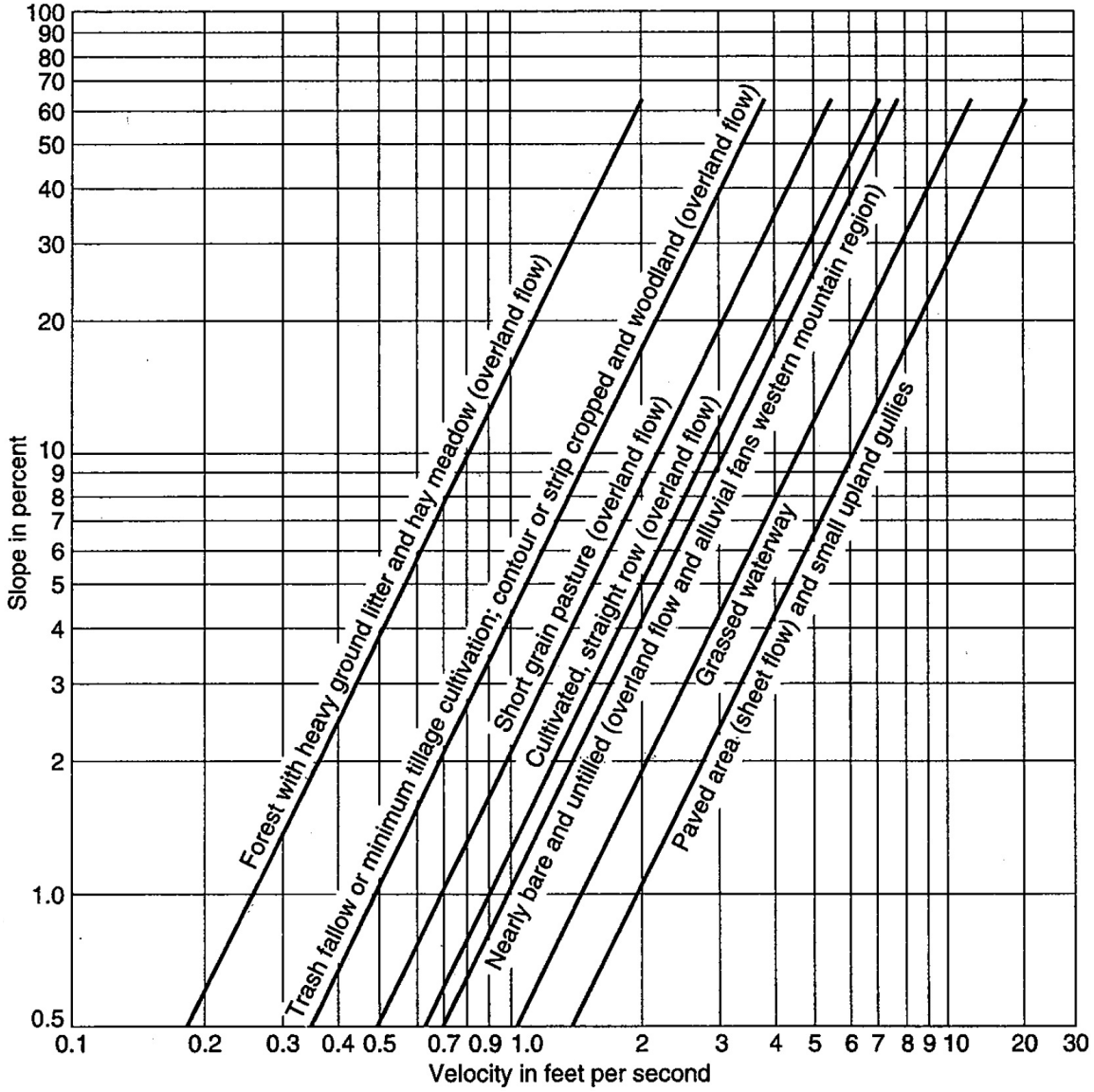

Figure **G-1**: Velocities for overland flow depending on land use and slope (Source: U.S. Soil Conservation Service, 1986

Appendix H

Statistical Significance of Seasonal Stream Temperature Changes

To determine whether the stream temperature response to spring storms is significantly different than the stream temperature response to fall storms, we completed a two-sample t-test assuming unequal variances. We split the 87 observed storms into two groups: spring storms occurred between April 3 and June 24, while fall storms occurred between June 25 and September 15 (all dates in 2011).

Table **H-1**: Summary statistics for data used in two-sample *t*-test

	Response to Spring Storms	**Response to Fall Storms**
Number of Observations	56	31
Mean of Group	0.035	-0.351
Variance of Group	0.72	0.58

For this t-test, our null hypothesis was that there was no statistically significant difference between how the stream temperature responds to the seasonal storms.

Table **H-2**: Results of two sample *t*-test

t-Test Parameter	**Value**
t Stat	2.175
p (T <= t) one-tail	0.017
t Critical one-tail	1.668
p (T <= t) two-tail	0.033
t Critical two-tail	1.995

Because the *p*-values (both one-tail and two-tail) from the t-test are below 0.05, we can reject the null hypothesis. This rejection means that the difference between these two groups is statistically significant.

Appendix I

Separation Bases for Investigating Runoff Sources

Table **I-1**: A sampling of recent field studies of runoff mechanisms (Source: Dingman, 2008).

Location	Mechanisms	Separation Basis	Source
Upland forest, Pennsylvania	Ground-water mounding; pressurization of capillary fringe; minor channel precipitation	^{18}O	Swistock et al. (1989)
Upland forest, Georgia	Sloping slab (mineral soil); sloping slab (organic soil); ground-water mounding	Six chemical constituents	Hooper et al. (1990)
Gently sloping forested hillside, Australia	Sloping slab (macropores)	^{2}H; Cl^{-1}	Leaney et al. (1993)
Coastal Plain, Virginia	Saturation overland flow	Cl^{-1}	Eshleman et al. (1993)
Forested swamp, Ontario, Canada	Saturation overland flow; ground water (macropore flow)	^{18}O, Cl^{-1}, Li^{+1}	Waddington et al. (1993)
Forested upland, deep soils, Tennessee	Bedrock (dolomite) ground water; ground-water mounding; sloping slab	Flow measurement; Ca, SO_4	Mulholland (1993)
Upland unforested watershed, Scotland	Hortonian overland flow; sloping slab; ground water	ANC[a]	Giusti and Neal (1993)
Forest and pasture watershed, Switzerland	Saturation overland flow; ground water; Hortonian overland flow	^{18}O	Jordan (1994)
Upland forest, Virginia	Saturation overland flow; subsurface flow	^{18}O, Cl^{-1}	Bazemore et al. (1994)
Tropical rain forest, Australia	Saturation overland flow; sloping slab; ground-water mounding	K^{+1}, ANC[a], ^{18}O, DOC[b]	Elsenbeer et al. (1995)
Shallow-soil forest, Canadian Shield	Saturation overland flow; sloping slab		Peters et al. (1995)
Mixed-forest, New Brunswick, Canada	Ground water	Conductivity, Alkalinity, pH, Na^{+1}, Mg^{+2}, Ca^{+2}	Caissie et al. (1996)
Unforested permafrost watershed, northern Alaska	Water tracks[c]	Conductivity, ^{18}O	McNamara et al. (1997)
Steep forested slope, Japan	Sloping slab	Flow measurement; tensiometers	Tani (1997)
Catskill Mts., New York	Sloping slab; ground-water mounding	Several solutes	Evans et al. (1998)
Steep, forested watershed, Maryland	Subsurface flow; channel precipitation	^{2}H, ^{18}O, Cl^{-1}, SiO_2, Na^{+1}	Rice and Hornberger (1998)

[a]Acid-neutralizing capacity

[b]Dissolved organic carbon.

[c]Subsurface "channels" of enhanced soil moisture that conduct flow directly downslope to streams.